12-2014

Development and Modeling of a Biosensor Platform using AlGaN/GaN HEMT Devices

Fahmida Shaheen Tulip
University of Tennessee - Knoxville, ftulip@vols.utk.edu

To the Graduate Council:

I am submitting herewith a dissertation written by Fahmida Shaheen Tulip entitled "Development and Modeling of a Biosensor Platform using AlGaN/GaN HEMT Devices." I have examined the final electronic copy of this dissertation for form and content and recommend that it be accepted in partial fulfillment of the requirements for the degree of Doctor of Philosophy, with a major in Electrical Engineering.

Syed K. Islam, Major Professor

We have read this dissertation and recommend its acceptance:

Jayne Wu, Gong Gu, Ramki Kalyanaraman

Accepted for the Council:
Carolyn R. Hodges

Vice Provost and Dean of the Graduate School

(Original signatures are on file with official student records.)

Development and Modeling of a Biosensor Platform using AlGaN/GaN HEMT Devices

A Dissertation Presented for the
Doctor of Philosophy
Degree
The University of Tennessee, Knoxville

Fahmida Shaheen Tulip
December 2014

Dedicated to

My parents
Dr. A. K. M. Shamsuddin
Asia Khatun

My better half
M. Shahriar Jahan

My sisters
Farzana Shirin
Farhana Sharmeen

Acknowledgements

First of all, I would like to express my heartfelt gratitude to Dr. Syed Kamrul Islam, my major advisor. Without his support, his guidance, and his encouragement this work would have been impossible. Special thanks go to Dr. Jayne Wu, Dr. Gong Gu, Dr. Ramki Kalyanaraman for serving in my committee and for reviewing my work.

I am grateful to Dr. Edward Eteshola for giving me the opportunity work in the HEMT based biosensor which became the topic of my dissertation. I am also thankful to Dr. Ida Lee for her discussions regarding the workings photosystems I. Also the members of Oak Ridge National Laboratory, specially Dale Hensley, Nickolay Lavrik and Timothy McKnight for their valuable discussions and suggestions for fabrication and development of the VACNF based glucose sensor. Dr. Asif Khan of University of South Carolina provided the HEMT devices used for testing purposes in this thesis and made the work possible. Dr. Muhammad Seraj Uddin and Dr. Shahinur Rahman of UTK also helped me by providing some necessary chemicals and equipment for test set-up.

I am also grateful to the present and past members of the Analog, VLSI and Devices Laboratory in UTK for their continuous support and valuable guidance. Specially Dr. Sazia Eliza, Dr. Hasina Haque, Dr. Touhidur Rahman, Dr. Salwa Mostafa helped me throughout various stages of my research. Dr. Kai Zhu, Dr. Melika Roknsharifi, Dr. Ashraf Islam, Dr. Aminul Haque, Terence Randall, Kimberly MacArthur, Logan Taylor, Ifana Mahbub, Farhan Qayium, Tan Yang, Nicholas Poore, Sanjib Das, Habib Ullah Habib, Khandaker Abdullah Al Mamun made my time in UT a pleasant and worthwhile one.

I am also thankful to the faculty and stuff of the EECS department in UTK, specially Dr. Nicole Macfarlane, Dr. Tolbert, Dr. Paul Crilly, Dr. Ortal Arel, Ms. Dana Bryson and Ms. Julia Evans for their continuous support.

Last but not the least; I would like to thank my family members, my parents, my husband and my sisters, who always had faith in me.

Abstract

The history of biosensors began in 1962 with the invention of enzyme electrodes by Leland C. Clark. Since then, biosensors have come a long way with simultaneous contributions in various fields such as biology, chemistry, material science, electronics, physics and VLSI. With the advancement in science and technology, smaller, more sensitive and dependable biosensors have become a reality. Still the need for cost-effective, sophisticated, reliable, robust biosensors that can be used to detect multiple types of biomolecules remains a technological challenge to be resolved.

The proposed AlGaN/GaN High Electron Mobility Transistors (HEMTs) have excellent prospect to become the biosensor platform of the future, as is investigated in this work in contrast to other types of biosensors. These devices excel over their silicon counterparts because of their inherent properties such as chemically stable bulk and surface properties and the availability of high-density two-dimensional electron gas (2DEG) at the hetero-interface which allows a highly sensitive detection of the surface-charge related phenomena. Using a floating gate configuration, only the drain current changes pertinent to biomolecule immobilization are observed. The test results are correlated with an analytical model which provides insight into the device physics. The high mobility and sensitivity inherent in its material system as well as device structure, robustness due to wide bandgap and system-level advantages make it the ultimate choice as a biosensor platform.

Table of Contents

List of Figures

Chapter 1

Introduction

1.1 Introduction

The demand for diagnosing and monitoring of chemical and biomolecular analytes are increasing day by day. Fast, reliable, ultrasensitive, portable sensor systems are of utmost importance for detecting these analytes. Particularly, electrochemical biosensors demonstrate relative simplicity, portability, low cost and low power requirement which make them excellent candidates for detecting a wide range of species, including proteins, nucleic acids, small molecules and viruses. Because of the recent trend of point of care application, this class of biosensors is rapidly becoming an important diagnostic tool. By incorporating integrated systems, carefully optimized functionalization of the sensor is supported by associated electronics, fluidics and separation technology. The potential for an extensive breakthrough of biosensor platform technology is a real possibility.

This chapter describes the motivation and objective of the research and summarizes the outline of the dissertation.

1.2 Motivation of Research

Modern day sensors have come a long way from their predecessors, which used transistors realized in bulky semiconducting materials. Advent of micro-fabrication technology has led to the miniaturization of biosensors. However, biosensors market is still characterized by slower pace of commercialization, which is primarily attributed to high cost, availability of effective alternative technologies, and issues related to stability, sensitivity, and quality assurance. Biosensors in medical and environmental applications still remain a hugely untapped market, attracting researchers as well as entrepreneurs, with the hope of leveraging dormant market opportunities.

Potential applications of biosensors include:

1. Food analysis
2. Study of biomolecules and their interaction
3. Drug development
4. Crime detection
5. Medical diagnosis (both clinical and laboratory use)
6. Environmental field monitoring
7. Quality control
8. Industrial process control
9. Detection systems for biological warfare agents
10. Manufacturing of pharmaceuticals and replacement organs

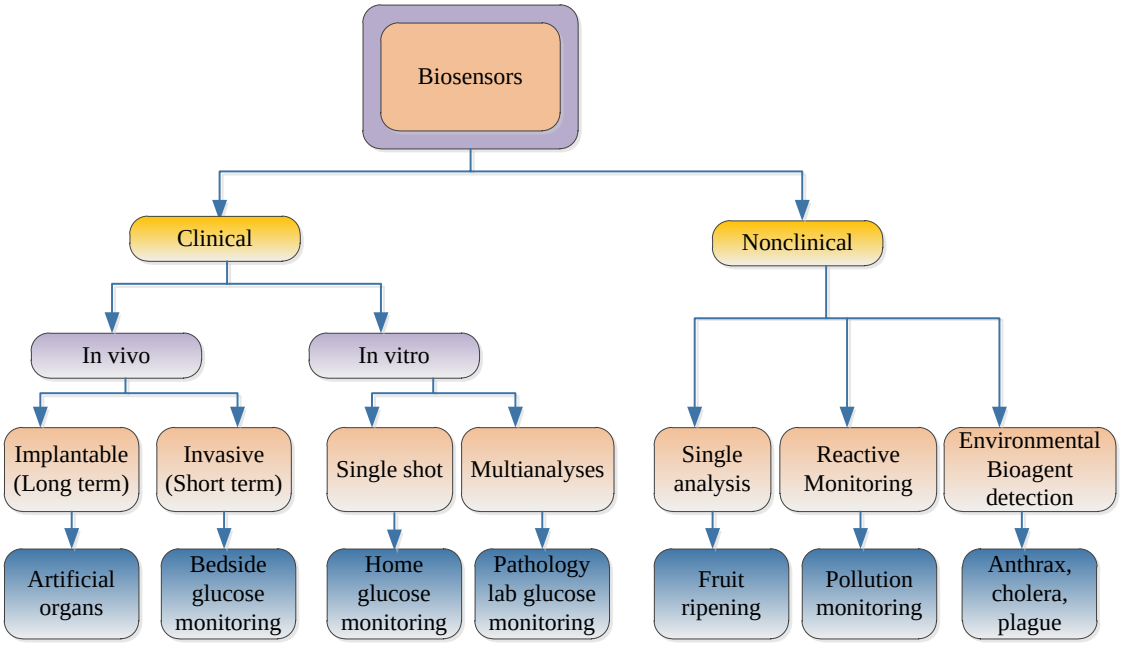

Figure 1.1: Potential applications of biosensors.

The global market for biosensors is projected to reach US $18.9 billion by the year 2019 from US $9.9 billion in 2012, at a compound annual growth rate of 9.6% [1]. Recent trends show that medical applications remain the dominant field in the global market for biosensors. Percentage revenue in worldwide biosensor market is shown in Figure 1.2.

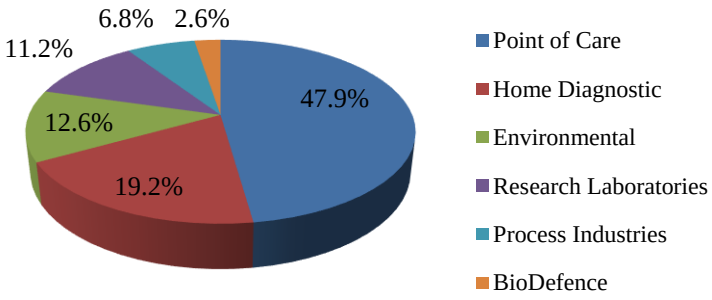

Figure 1.2: Global biosensor market in 2009 [2].

A robust, sensitive, cost effective biosensor platform can reap the benefits of leading the way in this emerging field. The proposed AlGaN/GaN high electron mobility transistors as investigated in this work have excellent prospect of becoming the biosensor platform of the future in contrast to other types of biosensors. Its high mobility and sensitivity inherent in its material system as well as device structure, robustness due to wide bandgap, and system level advantages makes it the ultimate choice for biosensor device.

1.3 Biosensors

According to International Union of Pure and Applied Chemistry (IUPAC), a biosensor is a self-contained integrated device that is capable of producing specific quantitative or semi-quantitative analytical information using a biological recognition element which is in direct contact spatial with a transducing element.

A biosensor uses specific biochemical reactions to detect chemical compounds in biological samples. It comprises verily of two elements: a biological recognition element that interacts with the target analyte, and a transducing element that converts the recognition event into measurable signal.

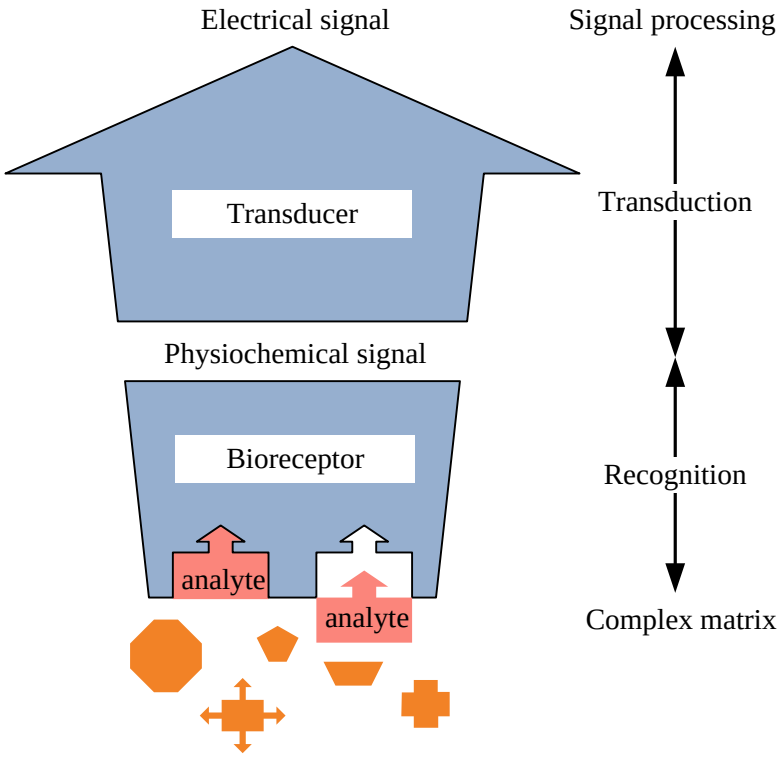

Figure 1.3: Components of a biosensor.

In a biosensor, the biological recognition element is immobilized in the vicinity of the transducing element, which is known as functionalization. This immobilization can be done by physical entrapment of chemical attachment. Immobilized biological recognition element attracts specific target analyte, and the recognition event is converted into measurable signal via transducer. The transducer might then send the signal further signal processing unit.

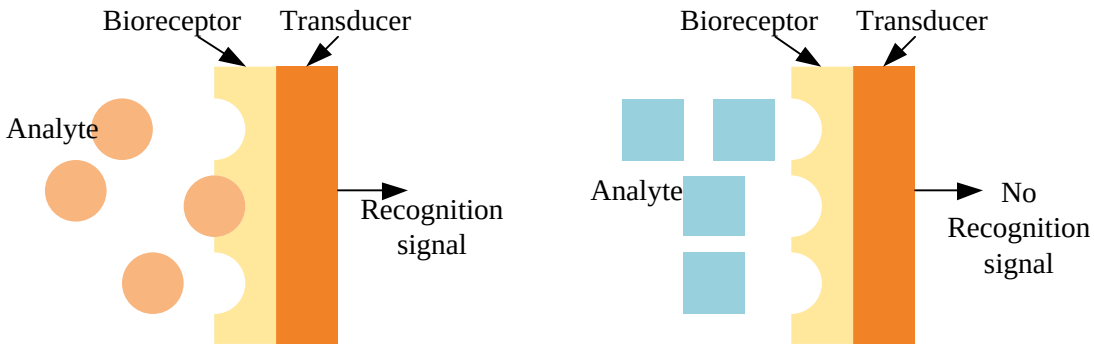

Figure 1.4: Specific recognition using biological recognition element is the basic of biosensor.

Sensitivity and selectivity are the two most important performance factors in a biosensor. A biosensor must be selective enough to ensure specific detection, as well as highly sensitive to convert the biorecognition event into useful measurable signal. The selectivity is ensured by using proper bioreceptors for functionalization, while sensitivity largely depends on the choice of device type used.

1.4 Research Objectives

As described in the previous sections, a suitable, robust, sensitive biosensor platform that can be used for multiple biomolecules can go a long way in the fairly untapped biosensor market. This work investigates the prospect of AlGaN/GaN HEMT as a biosensor in comparison with two other types of biosensor platform, namely nanofiber based biosensors and cantilever based biosensors. The superiority of the HEMT based biosensors over the other two types has been demonstrated. A physics based model to predict the behavior of the proposed bioFET is proposed to be developed. The model is validated using experimental data. The existing models of AlGaN/GaN HEMT found in the literature [3, 4] can be also be improved by considering the effects of polarization which serves as the key mechanism to induce the carriers in AlGaN/GaN HEMT devices. The physics based model is then modified for floating gate configuration to predict the behavior of the proposed HEMT based biosensor platform.

1.5 Outline of Dissertation

The second chapter of the dissertation contains the literature review on the history and types of bioFET. Chapter 3 presents two biosensor platforms which have been physically realized, and their pros and cons. Chapter 4 describes the advantages of HEMT device as a bioFET along with experimental data. Chapter 5 contains the charge control model of the proposed HEMT device, while chapter 6 describes the floating gate model of the device when configured as a bioFET. Original contributions and future work outlines are discussed in Chapter 7.

Chapter 2

Literature Review

2.1 Introduction

Technological advancement heavily relies on the estimation, monitoring and control of relevant chemical species. A major portion of this intelligence is acquired via sophisticated central laboratories. Nonetheless portable, sensitive and readily available sensor platforms are required in many circumstances, especially in clinical applications, where timeliness in both testing and monitoring of analytical markers are critical for diagnosis of the disease and patient treatment.

This chapter focuses to give a brief review of biosensor technology over the last five decades. Different types of biosensors, their desirable features and challenges that impede the advance in this field are also discussed.

2.2 A Brief History of Biosensors

L. C. Clark Jr., the father of the biosensor concept, first described a biosensor platform based on oxygen electrode in 1956 [5]. In 1962, he proposed an efficient method to make electrochemical sensors (pH, polarographic, potentiometric or conductometric) by introducing enzyme transducers as membrane enclosed sandwiches. The concept was illustrated by trapping glucose oxidase at a Clark oxygen electrode using dialysis membrane and observing the oxygen concentration level. The decrease in measured oxygen concentration was proportional to glucose concentration. Clark's glucose sensor was first launched as a commercial sensor in 1973. But it became a commercial success in 1975 with the re-launch of the Yellow Springs Instrument Company (Ohio) glucose analyzer based on the amperometric detection of hydrogen peroxide.

Guilbault and Montalvo [6] were the first to detail a potentiometric enzyme electrode. They described a urea sensor based on urease immobilized at an ammonium-selective liquid membrane electrode. The use of thermal transducers for biosensors was proposed in 1974 and the new devices were christened thermal enzyme probes [7] and enzyme thermistors by Mosbach [8], respectively. In 1975, Divis [9] suggested that bacteria could be harnessed as the biological element in microbial electrodes for the measurement of alcohol.

Lübbers and Opitz [10] coined the term optode in 1975 to describe a fiber-optic sensor with immobilized indicator to measure carbon dioxide or oxygen. They extended the concept to make an optical biosensor for the continuous measurement of chemical concentrations in a biological system using a fiber-optic oxygen sensor [11]. Commercial optodes exhibit excellent performance for *in vivo* measurement of pH, pCO_2 and pO_2, but enzyme optodes were not yet widely available. In 1976, Clemens *et al*. [12] incorporated an electrochemical glucose biosensor in a bedside artificial pancreas and this was later marketed by Miles (Elkhart) as the Biostator. Although the Biostator is no longer commercially available, a new semi-continuous catheter-based blood glucose analyzer has recently been introduced by VIA Medical (San Diego). In the same year, La Roche (Switzerland) introduced the Lactate Analyzer LA 640 in which the soluble mediator, hexacyanoferrate, was used to shuttle electrons from lactate dehydrogenase to an electrode. Although this was not a commercial success at the time, it turned out in retrospect to be an important forerunner of a new generation of mediated-biosensors and of lactate analyzers for sports and clinical applications. A major advance in the *in vivo* application of glucose biosensors was reported by Shichiri *et al.* [13] who described the first needle-type enzyme electrode for subcutaneous implantation in 1982. The idea of building direct immunosensors by fixing antibodies to a piezoelectric or potentiometric transducer had been explored since the early 70's, but it was a paper by Liedberg *et al.* [14] that paved the way for commercial success. They described the use of surface plasmon resonance to monitor affinity reactions in real time. The BIAcore (Pharmacia, Sweden) launched in 1990 is based on this technology. In 1984, a method was described to use ferrocene and its derivatives as an immobilized

mediator for use with oxidoreductases [15] in the construction of inexpensive enzyme electrodes. This formed the basis for the screen-printed enzyme electrodes launched by MediSense (Cambridge, USA) in 1987 with a pen-sized meter for home blood-glucose monitoring.

Academic journals contain descriptions of a wide variety of devices exploiting enzymes, nucleic acids, cell receptors, antibodies and intact cells, in combination with electrochemical, optical, piezoelectric and thermometric transducers1, [16]. Within each permutation lies a myriad of alternative transduction strategies and each approach can be applied to numerous analytical problems in health care [17], food and drink [18], the process industries [19], environmental monitoring [20], defense and security. Generic goals may be identified which underpin more applied biosensor programs and tackle some of the principal hurdles to the more widespread adoption of biosensor technology for analysis. Design of integrated systems as well as approaches to patterning sensitive elements and methods for improving the sensitivity, stability and selectivity of the biosensors are the key areas of biosensor research.

2.3 Different Types of Biosensors

Biosensors comprise a combination of three building blocks: a biological or physiological system; instrumentation or sensing system; and an electrical and electronic system. The biological or physiological system refers to the preparation of the target analyte and modifying the sensor system for detection, the instrumentation or sensing system refers to the instrument, fitted with highly sensitive and accurate sensors, and the electrical and electronic system refers to the associate circuitry which manages the signal processing and the conversion to an analog/digital display.

Based on this basic platform, a number of different technologies have been developed to construct biosensors, not all of which are used in all application types. Figure 2.1 describes the key biosensor technologies that are currently in use. Different biosensors exploit different inherent properties such as physical, chemical, electrical, mechanical or optical properties of the sensing material.

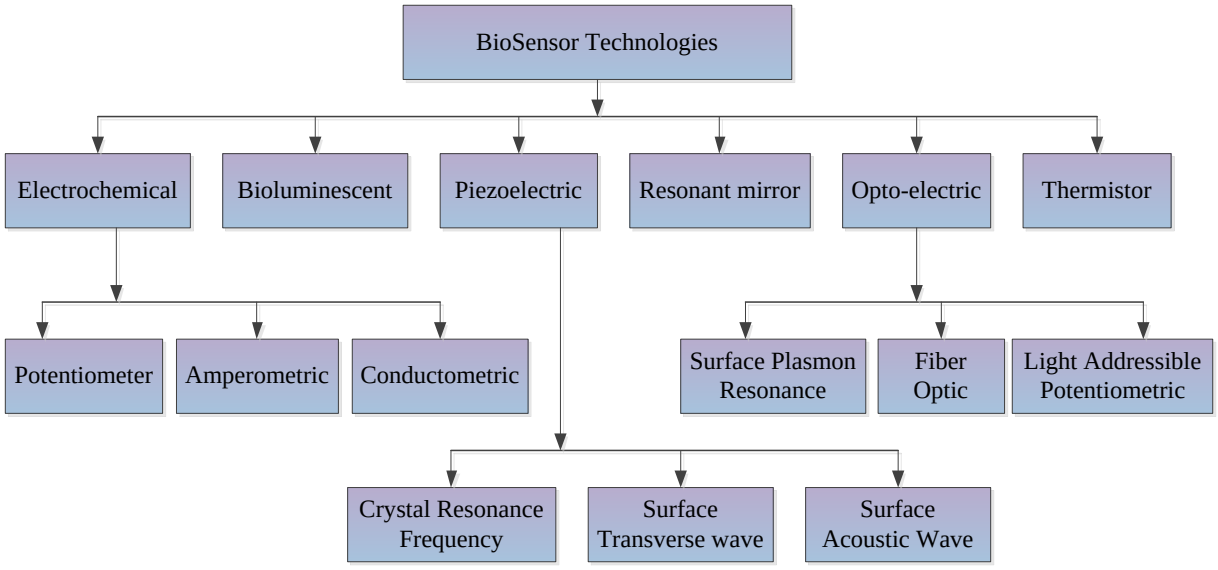

Figure 2.1: Different types of biosensors.

2.4 Desired Features of Biosensors

2.4.1 Sensitivity

Clinical applications, food technology and environment monitoring demand increased sensitivity and detection range for various analytes. While the precise demands to meet today's requirements may be modest in these respects, the long term benefits of reliable detection of trace amounts of various indicators, additives or contaminants is uncontended. With the advent of atomic force microscopy, single molecule detection in the research laboratory is possible, but great strides have also been made with conventional sensors for the detection of the analytes of interest. Enzyme electrodes have been designed which preconcentrate the target analyte [21]. A gas-phase microbiosensor has been reported for phenol in which polyphenol oxidase was immobilized in a glycerol gel on an interdigitated microelectrode array [22]. Ultra-low detection limits are achievable with affinity sensors and electrochemical detection may be readily integrated with chromatographic techniques to yield user-friendly devices [23]. In an alternative

approach, double-stranded DNA may be used as a receptor element. "Sandwich"-type biosensors based on liquid-crystalline dispersions formed from DNA-polycation complexes may find application in the determination of a range of compounds and physical factors that affect the ability of a given polycation molecule to maintain intermolecular crosslinks between neighboring DNA molecules [24].

2.4.2 Stability

The most obvious disadvantage in exploiting the exquisite specificity and the sensitivity of complex biological molecules is their inherent instability. Many strategies may be employed to restrain or modify the structure of biological receptors to enhance their longevity. The effectiveness of sol-gels as an immobilization matrix in an optode for glucose to enhance the stability of the glucose oxidase catalyst has been demonstrated [25]. Some desirable activities, however, remain beyond the reach of the current technology.

2.4.3 Selectivity

The selectivity of the biosensors can be improved by adopting two different methods; the interface between the transducer and the biological receptor may be made more exclusive thus reducing interference, and new receptors can be developed with improved or new affinities. The use of mediators as a strategy to improve performance in amperometric biosensors has also been proved extremely popular. Alternatively, electrocatalytic detection of the products of enzymatic reactions may be enhanced by the use of chemically modified electrodes such as rhodinised [26] or hexacyanoferrate-modified [27] carbon. Arguably a more elegant solution is to seek connection of the redox center of an enzyme to an electrode via a molecular wire. Much has been published about these "wired" enzymes, but the literature has generally been concerned with immobilized mediators on various polymer backbones. Novel heteroarene oligomers, consisting of two pyridinium groups, linked by thiophene units of variable length (thienoviologens) are promising candidates for such conducting molecular wires and may be used in conjunction with self-assembly techniques to produce an insulated electrode which transfers electrons

specifically along predetermined molecular paths [28]. This design should produce enzyme electrodes free from electrochemical interference. Advances in computational techniques now allow us to model both electron transfer reactions and receptor binding interactions with increasing accuracy. This not only enhances our understanding of the receptor/transducer interface, but allows us to consider designing new receptors based on biological molecules.

2.5 Challenges in Biosensor Technology

In spite of a number of innovative biosensors developed to date, the biosensors market is still far from meeting some of the key end-user needs. The key features that are yet to be implented include:

- development of biosensors capable of multitest detection and monitoring
- development of integrated biosensing platforms
- development of a self-configuring biosensor
- complete multiproduct, multivendor interoperability among biosensors
- migration to lab-on-chip biosensors
- availability of wireless options

There are various issues that hinder the growth of biosensor technology. To begin with, the lifespan of a biomolecule is usually limited which calls for rapid detection. The readout time greatly varies from one biosensor to another. In certain cases, the readout time can be as long as 20 seconds. Most biosensor requires chemical pre-treatment prior to any kind of detection, which slows down the detection process. Long term stability and miniaturization issues of the sensors still remain unsolved, which in term reduces the cost-effectiveness of the sensors for commercial applications. Moreover, most biosensing techniques require bulky optical instruments which are not suitable for point of care applications. Rugged biosensors that can work in extreme environments to monitor vital signs also have limited availability.

Considering all these technical challenges, it can be concluded that there is a great need for a portable, miniature, robust, sensitive biosensor platform.

Chapter 3

Electrode and Transistor Based Biosensor Platforms

3.1 Introduction

Biosensors were first developed based on electrode conduction principle. As such, most commercial biosensors found to date are also based on the similar technique. But to reap the benefits of inherent gain of transistors and to provide easy integration with data processing circuitry, transistor based biosensors are gaining more popularity nowadays. This chapter gives a description of two different types of biosensor platforms that has been tried with their working principle and experimental data collected. The first type is based on electrode conduction, where carbon nanofibers are used as electrodes. The second type is cantilever based, where the microcantilever at the base of a transistor is used for detection and the advantages of a transistor based system is also utilized.

3.2 Glucose Sensor Based on Vertically Aligned Carbon Nanofibers

Carbon electrodes have been proven successful when used as enzymatic biosensors in terms of wide range of functionality and cost effectiveness. Among the carbon electrodes carbon nanostructures (cylindrical or conical structures) demonstrate the best potential. These carbon nanostructures have diameters varying from a few nanometers to hundreds of nanometers and lengths ranging from less than a micron to a few millimeters [29]. Although carbon nanotubes (CNTs) have been widely used in biosensor research, carbon nanofibers (CNFs)are emerging as a potential candidate to replace CNTs. CNFs have excellent conductive and structural properties comparable with CNTs that make them excellent candidates as electrodes as well as immobilizing substrates[30], [31]. CNTs and CNFs can be used as electron field-emission sources, electrochemical probes, functionalized sensor elements, scanning probe microscopy tips, hydrogen and charge storage devices, catalyst support, and nanoelectromechanical systems (NEMS). Only the tips of the CNTs are active owing to their extremely regular shapes. In contrast, a CNF has many irregularities and defect sites with exposed carboxyl groups throughout their

surfaces, which serve as excellent locations for electrochemical charge transfer [32]. These result in better sensitivity and responsiveness in the CNFs compared to the CNTs [33]. Because of superior structural properties the CNFs also have better mechanical stability than the CNTs [34].

Because of the clinical significance, substantial research and development efforts have been devoted to the development of reliable glucose sensors. Most of the proposed glucose sensors rely on amperometric enzyme electrodes based on glucose oxidase (GOx).Oxidase based biosensors depend on the immobilization of the oxidase enzymes and the co-enzymes on the surface of the electrodes and the subsequent detection of the current associated with the redox product in the biological reaction. Mediator based glucose sensors are also proposed in literature where artificial mediators and permselective coatings are introduced in biosensor fabrication to increase the selectivity and the sensitivity of the amperometric biosensors [35, 36]. Use of some of the mediators is limited by stability and toxicity while the permselective membranes show effective but incomplete rejection [37, 38].

An attractive way to improve the performance of the glucose sensor is to use an enzyme wiring technique. Enzyme wiring improves the electrical contact between the redox center of the electrode surfaces and glucose oxidase (GOx) [39]. Due to similar dimensions of the nanoparticles and the redox proteins such nanomaterials can be used for effective electrical wiring of redox enzymes. Various types of nanomaterials such as gold nanoparticles [40], carbon nanotubes (CNT) [41] have been used as electrical connectors between the electrodes and the redox centers of the GOx. Carbon nanotubes (CNT) can be coupled to the enzymes to provide a favorable surface orientation and can act as an electrical connector between their redox centers and the electrode surfaces. Patolsky et al. demonstrated that the aligned reconstituted GOx on the edge of the single-wall carbon nanotubes (SWCNT) can be linked to an electrode surface [41]. Various glucose biosensors based on CNT have been proposed taking the advantage of this excellent property of ‘plugging’ of the electrode with GOx [42], [43]. Due to their

superior sensitivity compared to CNTs, VACNFs can be easily used to build glucose biosensors based on this enzyme wiring technique.

3.2.1 Working Principle

In general the oxidase-based biosensors depend on the immobilization of oxidase enzymes and co-enzymes on the surface of the electrodes and the subsequent detection of the current associated with the redox product in the biological reaction. Total workflow of the proposed glucose biosensor system is shown in Figure 3.1.

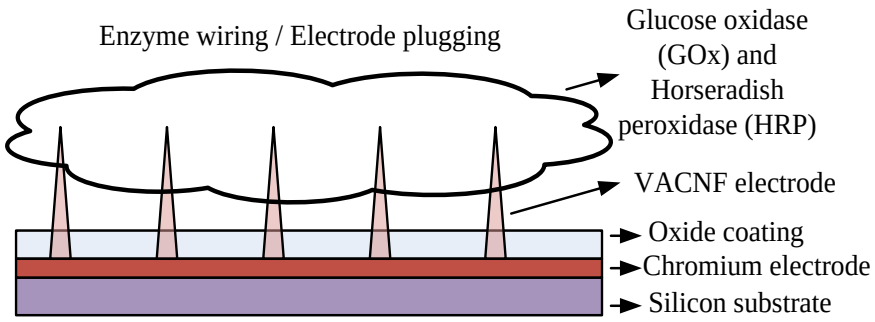

Figure 3.1: A cross sectional view of the fabricated VACNF based biosensor. The biosensor is prepared by co-immobilization of HRP and GOx on the VACNF surface. Chromium electrode was plugged with the GOx through VACNF by the enzyme wiring technique.

Initially GOx functions as an enzyme and binds the β-D-glucose on the VACNF/HRP/GOx electrode surface. Next the GOx catalyzes the oxidation process and transform β -D-glucose to D-glucono-1, 5-lactone, which is then hydrolyzed to gluconic acid:

$$Glucose + O_2 \xrightarrow{GOx} Gluconic\ Acid + H_2O_2 \quad (3.1)$$

The reduction process corresponds to the electrocatalytic reduction of hydrogen peroxide (H_2O_2) by the co-enzyme horseradish peroxidase (HRP) (equations 3.2 – 3.4) [43, 44]. The reduction reaction can be shown as:

$$H_2O_2 + 2H^+ + 2e^- \xrightarrow{HRP} 2H_2O \quad (3.2)$$

This reduction reaction can be divided into two reactions where HRP actively catalyzes the process [43, 44]:

$$HRP(Fe^{3+}) + H_2O_2 \rightarrow compound\_I + H_2O \quad (3.3)$$

$$compound\_I + 2e^- + 2H^+ \rightarrow HRP(Fe^{3+}) + H_2O \quad (3.4)$$

Hydrogen peroxide (H_2O_2) resulting in this process is used for the reduction reaction. HRP is a co-enzyme which has accessible active sites. As a result the electron donors and the acceptors can participate in the reaction where HRP plays the role of a catalyst. The reduction process corresponds to the electrocatalytic reduction of H_2O_2 by HRP produced by the oxidation process (see equations 2 - 4). Electrons required for the reduction process are supplied externally by the Cr electrode via VACNFs to the reaction centers. If the current associated with the flow of electrons due to the redox reactions can be measured, it can directly be correlated with the amount of glucose present in the biosensor system. Thus glucose detection is possible by measuring the reduction current only.

3.2.2 Experimental Setup

A bienzymatic biosensor is prepared by co-immobilizing HRP and GOx on the VACNF surface. To confine the chemicals to the area of interest, a well is formed around the nanofiber forests. The amounts of HRP and GOx are chosen in such a way that they can cover the entire surface area of the VACNF forest. Then the entire sensor chip is dried using a vacuum pump. When not in use all the modified

electrodes are stored at 4°C in phosphate buffer saline (PBS). The Cr electrode was plugged with the GOx through the VACNF via enzyme wiring technique to facilitate an efficient way to transfer electrons from the electrode to the reaction centers. A CHI 666A electrochemical analyzer was used for measurement. The tungsten working electrode (cathode) was connected to the VACNF and the tungsten reference electrode (anode) and the counter electrode were connected to the solution, as shown in Figure 3.2.

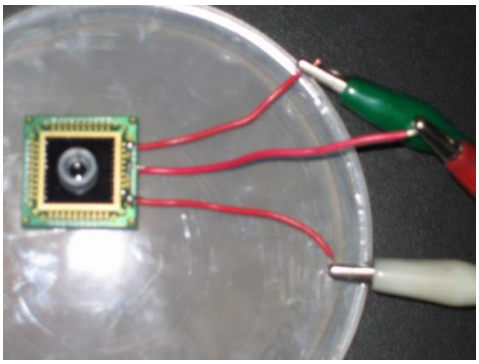

Figure 3.2: Test setup for the glucose sensor using VACNF electrode.

3.2.3 Results and Discussion

Figure 3.3 represents the amperometric response of the VACNF/HRP/GOx glucose sensor. In the absence of glucose, application of a potential between the electrodes results in a current flow between them. Addition of glucose to the system induces a flow of reduction electrons, which opposes the initial flow of current. This is represented by the overall decrease in measured current. This result is similar to the result reported by Wu *et al*. [38].

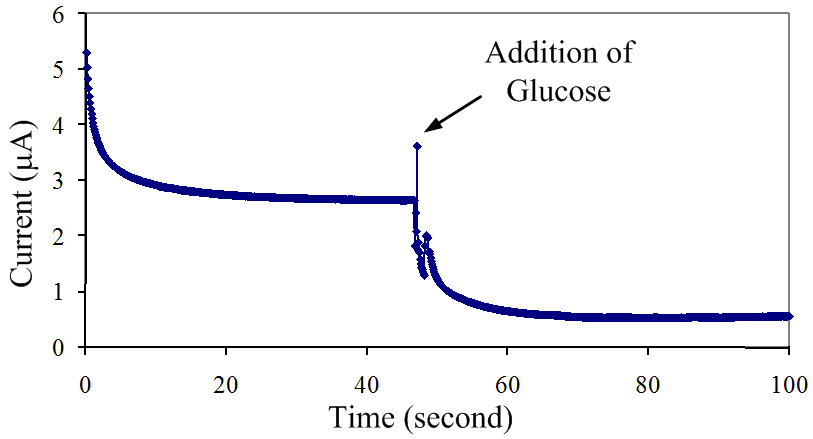

Figure 3.3: Amperometric response of VACNF/HRP/GOx biosensor in 0.1 M pH 7.4 PBS in the addition of 4 mM glucose. The biosensor responded immediately with the addition of glucose. Initial potential was set to -0.4 V.

3.3 Anthrax Sensor Based on Microcantilever

Microorganisms have been in existence for billions of years and their importance in environmental processes and human activities is well recognized. Certain bacteria, notably those of the Bacillus and Clostridium groups, differentiate spores that are highly resistant to chemical and physical insults. Spores of these certain species demonstrate persistent attachment to inert and negatively charged surfaces. Development of a lightweight and spore-specific sensor is very useful for early detection of the presence of bacterial spores.

Biomolecule detection can be achieved by the immobilization of biomolecules on a chemically treated cantilever which affects the performance of the embedded MOSFET. Targeted binding of the biomolecule generates stress on the cantilever which creates interface defects and traps in the channel region of the embedded MOSFET, thereby reducing mobility. Different designs including the orientation of the cantilevers with respect to the embedded MOSFET have been adopted to maximize the stress effects on the characteristics of the MOSFET [46].

3.3.1 Working Principle

For the cantilever along the transversal direction of the current flow in the MOSFET [47], the transverse tensile stress dominates the compressive longitudinal stress. The change in the channel resistance due to the applied stress can be written as [46],

$$\frac{\Delta R}{R} = \pi_t \sigma_t + \pi_l \sigma_l$$

Here the subscripts *t* and *l* stand for transverse and longitudinal directions, respectively. The combined effect of the variations of the piezoresistive coefficients ($-\pi_t$, $+\pi_l$) and the stress components ($-\sigma_t$, $+\sigma_l$) in the cantilever due to the adsorption of target molecules results in increased channel resistance (reduced mobility) and therefore reduced drain current. Overall, the embedded structure shows high sensitivity (1-2 μA/nm) enabling the detection of 5 to 10 nm deflections of the cantilever [47].

3.3.2 Experimental Setup

Microcantilevers are fabricated as arrays, where cantilevers of SiN_x and SiN_x with thin gold coated layer are placed in an alternating fashion. The embedded MOSFETs are located at the base of the cantilevers where stress due to adsorption is the maximum.

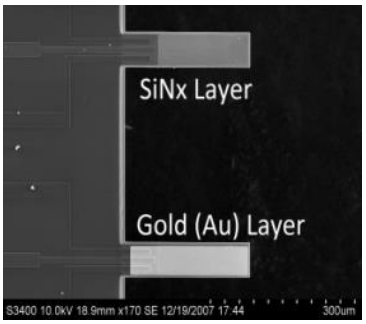

Figure 3.4: SEM image of two identical cantilevers displaying embedded MOSFET and geometry of the gold-coated and SiN_x cantilever beam pair [47].

For microbial sensor a MOSFET at the base of a SiN_x microcantilever works as the reference whereas a MOSFET at the base of a SiN_x microcantilever with a thin coating of gold is used as the probe as shown in Figure 3.4. The differential drain current between the probe and the reference microcantilevers, which further minimizes systematic noise and environmental perturbations, forms the basis for the anthrax simulant detection due to selective adsorption to the gold-coated probe.

For the experiments, the MOSFET-embedded microcantilevers were first characterized to obtain the drain current versus the drain-to-source voltage curves to be used as reference as shown in Figure 3.4. Then, both the bare SiN_x and the gold-coated cantilevers were submerged in a phosphate buffer solution (PBS) to chemically treat the cantilevers for anthrax simulant attachment. Effect of the buffer solution application was observed by taking the characteristic curves of both MOSFETs. Afterwards 15µL of anthrax simulant solution (suspension population of 1.3×10^7 Colony Forming Unit/ml diluted in 40% ethanol and 60% de-ionized water) was applied over the cantilever MOS pairs in doses of 5µL. Characteristic curves were obtained after each dose application. Under the microscope the bending of the gold-coated cantilever was clearly visible whereas the silicon nitride cantilever remained unaffected. It was noticed that the anthrax simulant spores were attracted to the voltage supplying probes when voltage was applied to obtain characteristic curves. Signatone Checkmate probe station and HP 4155B parameter analyzer were used for collecting the measurement data.

3.3.3 Results and Discussion

Before the application of phosphate buffer solution (PBS) both the SiN_x and gold-coated cantilever MOS structures demonstrate similar characteristic curve as shown in Figure 3.5a. Application of PBS causes the gold cantilever to bend as it gets attached to the gold surface while SiN_x cantilever remains unbent. The effect of applying PBS on the MOSFET drain current, as one cantilever bends and the other remains unbent is shown in Figure 3.5b.

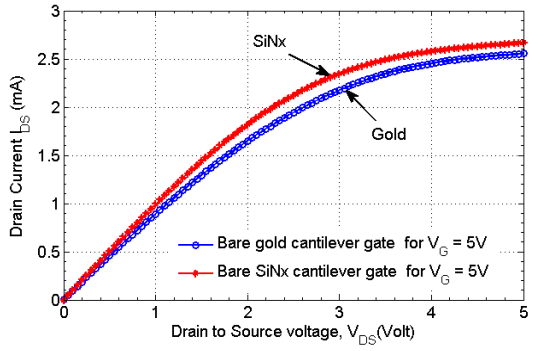

(a)

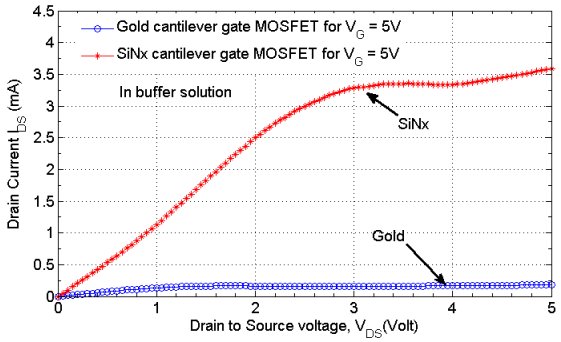

(b)

Figure 3.5: a) Characteristic curves of SiN_x and gold coated cantilever MOS at applied gate voltage of V_G = 5V, b) responses of Au and SiN_x MOSFETs with V_G = 5V in buffer solution.

Due to selective adsorption, anthrax stimulant adhere to only the gold-coated cantilevers and probe MOSFET experiences stress and subsequent drain current reduction phenomenon. SiN_x cantilevers do not adhere to biomolecules, therefore the reference MOSFET do not show any change in current.

3.4 Conclusion

Although both the VACNF and microcantilever based sensors provide promising results, they fail to provide for the demands of the rugged, simplistic biosensors that can be commercialized, at least at their current state of development. Nanofiber based sensors require complex imprint technology, and the integration with CMOS circuitry is also difficult. Microcantilever based sensors can utilize the benefits of

transistor based systems and can be readily integrated with CMOS circuitry for signal processing, but they lack mechanical stability and thus cannot be used for high concentration biomolecule samples. The target biomolecules must be diluted, thereby requiring an extra step in the sensing process. Also, since they use strain on the cantilever, they are more susceptible to give a false alarm if some dust or unwanted particles falls on the cantilevers. As such, there still remains the need for a truly transistor based system where the biomolecules will interact with the sensor electrically.

Chapter 4

High Electron Mobility Transistor as BioFET Platform

4.1 Introduction

In this chapter, the advantages of AlGaN/GaN high electron mobility transistor (HEMT) as a bioFET are explained. While compared to the biosensor platforms presented in chapter 3, the HEMT based biosensor platforms demonstrate chemical and surface stability, high sensitivity towards surface charge phenomena to become the ultimate choice. Two different types of biomolecules, one from plant (photosystem I, or PS I) and one from human body (Human Monokine induced Interferron Gamma, or human MIG) are detected by the HEMT devices configured as biosensor. The experimental data shows excellent promise to differentiate between the presence and absence of target biomolecules.

4.2 HEMT Structure

Of the various device FET structures, HEMT devices show better performance as high-power and high-frequency devices. Capacitive modulation of the channel charges is the basic principle of operation for all the FET devices. With this common concept, use of different geometries, different materials and doping profiles results in the variety of FET transistors. Eventually, each type of FET would differ in the confinement of the channel charges and the isolation between the gate and the channel, which would result in a novel device with specific properties. The first HEMT was based on GaAs/AlGaAs superlattices pioneered by L. Esaki and R. Tsu at IBM in the late 1960's [48]. They proposed that by modulation doping, a process where electrons are transferred from highly doped and wider bandgap material (AlGaAs) to a lightly doped material (GaAs), high mobilities in GaAs is achieved [48]. R. Dingle, H. L. Stormer, A. C. Gossard, and W. Wiegmann of AT&T Bell Labs, working independently, demonstrated high mobilities in a GaAs-AlGaAs superlattice in 1978. Realizing the high performance capability of such a structure of the field-effect transistor, researchers of various labs in the United States (Bell Labs, University of Illinois, and Rockwell), and Japan (Fujitsu), and France (Thomson CSF) started

working on this device. In 1980, the University of Illinois and Rockwell first fabricated such a device with a reasonable microwave performance, which they named as modulation-doped FET or MODFET. The same year researchers at Fujitsu reported the results for a device with a 400-pm gate. They called the device “high electron mobility transistor” or HEMT. Thereafter, Thomson CSF and Bell Labs followed calling their realizations a “two-dimensional electron gas FET” or TEGFET, and “selectively doped heterojunction transistor” or SDHT, respectively [48].

In conventional metal-semiconductor FET’s (MESFET’s), the donor impurities generate the electrons (carriers) and reside in the same space/layer with the electrons. As a result, the conducting electrons start colliding with the impurities. For higher speed, more current is required which necessitates larger concentration of electrons. This leads to more electron-donor interaction, called ionized impurity scattering.

In addition, thinner channel layers and higher electron concentrations are required for smaller FET size. The isolation of large electron concentration with donors can be obtained by employing heterojunctions. A heterojunction is formed between two different bandgap materials such as AlGaAs and GaAs. The donors are introduced only into the larger bandgap (AlGaAs) material [49], [50]. The electrons originally introduced into the larger bandgap layer (AlGaAs) diffuse to the lower energy (GaAs) layer where they remain confined due to the energy barrier at the heterointerface as illustrated by the band diagram in Figure 4.1.

Thus, a 2-dimensional electron gas (2-DEG) is formed at the heterointerface very close to the gate, which leads to very high electron mobilities and large electron velocities at very small values of drain voltage [51].

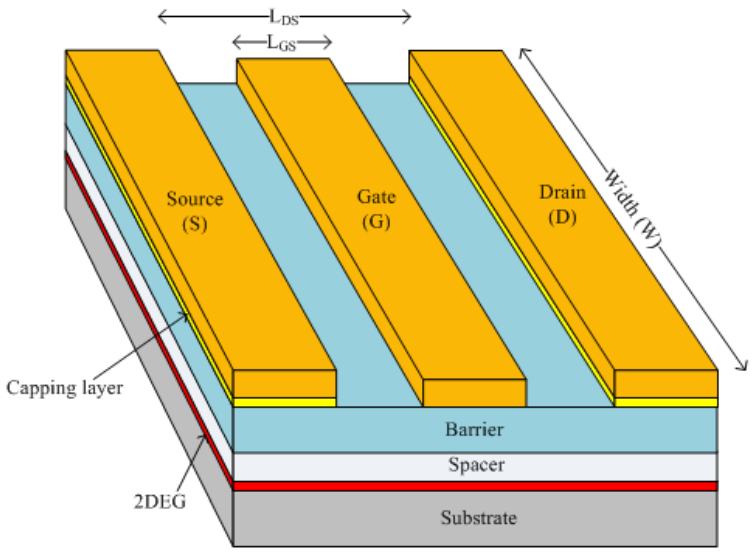

(a)

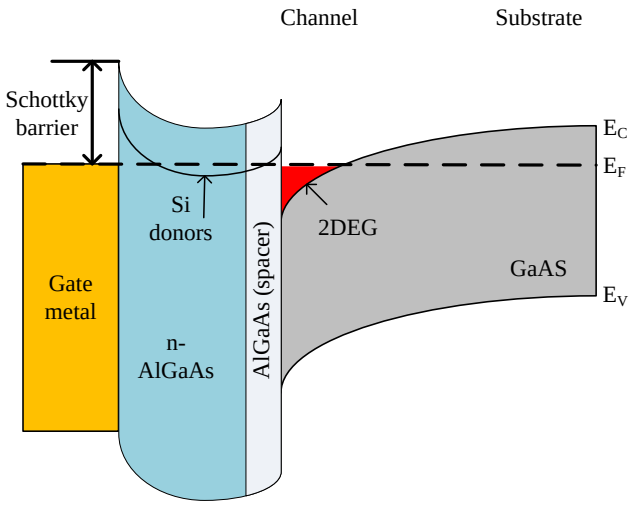

(b)

Figure 4.1: (a) Schematic diagram of an AlGaAs/GaAs HEMT structure, (b) Energy band diagram of the HEMT device showing the formation of the 2 dimensional electron gas in the quantum well.

In 1993, Asif Khan et al. first demonstrated a HEMT based on AlGaN and GaN heterojunctions [52]. Since then much progress has been made for the achievement of better performances of AlGaN/GaN HEMT. AlGaN/GaN exhibits improved ratings for power and frequency applications compared to AlGaAs/GaAs HEMT. This is due to the superior intrinsic properties of GaN material compared to GaAs as evident from Table 4.1 and also due to the polarization effects dominant in AlGaN and GaN materials.

Table 4.1

Comparison of Different Semiconductor Materials

Semi-Conductor	E_g ***(eV)***	μ ***(cm^2 / V-sec)***	ε_r	E_c ***(kV/ cm)***	v_s ***(10^7 x cm/sec)***	λ ***(W/cm-K)***	T_{max} ***(^oC)***
Si	1.1	1300	11.4	300	1	1.5	300
GaAs	1.4	5000	13.1	400	1	0.46	300
SiC	2.9	260	9.7	2500	2	1.49	600
GaN	3.4	1500	9.5	2000	2.2	1.3	700

GaN has both Zincblende nad Wurtzite crystalline forms. It is normally grown on the Ga-face, along its c-axis. It has a substantial spontaneous electrical polarization perpendicular to the hexagonal plane, and in the direction down into the Ga-face surface. When $Al_xGa_{1-x}N$ is grown on GaN, larger electrical polarization results in the same direction. $Al_xGa_{1-x}N$ has a smaller lattice constant, so that the two-

dimensional tension causes a piezoelectric effect which adds to the spontaneous polarization [53]. A positive sheet charge density appears due to the net polarization effect, which causes an accumulation of electrons at the interface and thus forms the 2-DEG as shown in Figure 4.2. Thus, even without any intentional doping in the AlGaN layer, a high charge density channel is formed at the heterointerface.

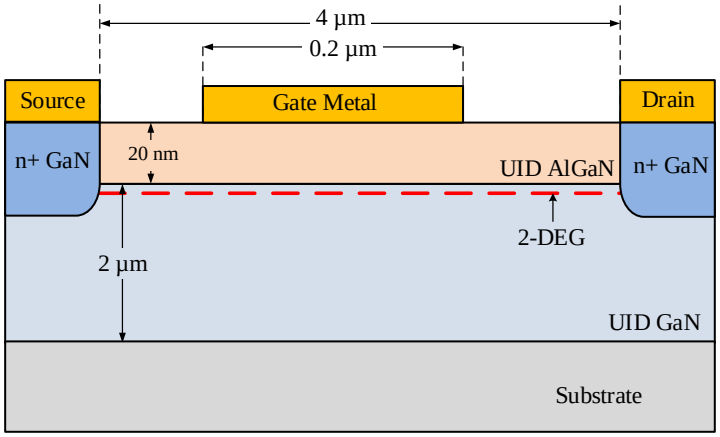

Figure 4.2: AlGaN/GaN HEMT structure and the formation of 2DEG.

4.3 Advantages of AlGaN/GaN HEMT as a BioFET

The AlGaN/GaN high electron mobility transistor (HEMT) devices are focus of increasing interest as biologically modified field effect transistor (BioFET) based micro- and nano-electronic sensor platforms in recent years. They excel over their counterparts because of their inherent properties such as: (i) chemically stable bulk and surface properties, (ii) a high-density two-dimensional electron gas (2DEG) available at the hetero-interface which allows a highly sensitive detection of surface-charge related phenomena, and (iii) as a piezoelectric material, its conductivity changes upon a change of the surface

charge, such as that due to binding of antigen onto an antibody-functionalized surface11. These very favorable material attributes significantly facilitate amplification of the current change pertinent to change in the gate potential due to the proximity of the immobilized biomolecules and/or biomolecular binding events between the charged biological molecules (e.g., antigen-antibody or receptor-analyte binding events) at the high charge density sensing channel or the gate surface [54,55].

4.4 Experiments

4.4.1 Photosystem I

PS I reaction centers are potential sources of solar energy. Using sunlight, these reaction centers generate electrical potentials which can be accumulated to build substantial source of electrical energy if proper extraction technique can be developed. In oxygenic plants there are two types of reaction centers – Photosystem I (PS I) and Photosystem II (PS II). Both of the reaction centers work in succession to produce glucose for green plants, some bacteria and protists in photosynthesis. Photosynthesis is a two phase process. The first phase is light dependent which requires direct energy of light to produce energy carrier molecules. The second phase is light independent. During the first phase, light energy induces electron separation in PS II. PS II fills the electron from a water molecule, breaking the water into H^+ ions and O^{-2} ions. These O^{-2} ions combine to form O_2 molecule. The electron is boosted to a higher energy state and finally transferred to PS I through electron acceptor and a series of redox reactions. The electron is again passed through a series of redox reactions and eventually becomes attached to $NADP^+$ and H^+ to form NADPH, which is the energy carrier in the light independent reaction. There is thus a continuous flow of electrons from water to NADPH, which is used for carbon fixation in the light independent process. Thus, PS I and PS II work as energy harvesting units in photosynthesis.

PS I RC/core antenna complexes containing about 40 chlorophylls per photoactive reaction center pigment (P700) can be isolated efficiently from thylakoids of plant leaves (such as spinach) using the

technique of detergent solubilization and hydroxylapatite column purification [56]. The isolated PS I complexes are elliptical in shape with major and minor axes of about 6 and 5 nm, respectively [56].

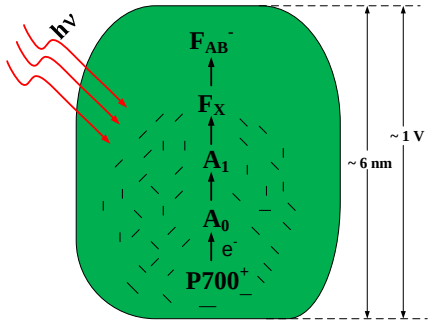

Figure 4.3: Charge separation in PS I due to absorption of light.

The structure and the function of PSI reaction centers are schematically illustrated in Figure 4.3. An isolated PS I complex contains photochemical charge center of P700 and electron acceptors of A_0, A_1, F_X and F_{AB}. These electron acceptors serve as an antenna to capture photons and transfer photon energy to P700.The light energy triggers photochemical charge separation in P700 creating $P700^+$ and A_0^- within about 1.5ps [57].The electron released from P700 is transferred through intermediate acceptors A_0, A_1, F_x, to the terminal acceptor F_{AB} at the reducing side of the PS I. Due to efficient excitation transfer and trapping, the entire photophysical chemistry can be completed in 10-30 ps. The quantum yield of PS I photochemistry is very close to 100%. Charge separation in this natural photovoltaic device generates a potential difference of about 1 volt across about 6 nm dimension between the reduced (F_{AB}^-) and the

oxidized ($P700^+$) sides of the PS I complex, resulting in a very strong electric field (~ -10^8 volts per meter).

4.4.1.1 Functionalization of the BioFET

Organic SAMs on solid surfaces are one of the most suitable functional linkage-layers for the immobilization of biomolecular complexes. To date, the SAMs of alkanethiols on Au surfaces are the most intensively studied immobilizing systems. Functional PS I RCs can be selectively immobilized and oriented by the chemical modification of the Au surface [56]. Two-dimensional vectorial arrays of functional PS I RCs have been prepared on atomically flat derivatized Au surfaces [56]. The atomically flat Au {111} substrate were treated with mercaptoacetic acid ($HSCH_2COOH$), 2-dimethylaminoethanethiol [$(CH_3)_2NCH_2CH_2SH$], and 2-mercaptoethanol ($HSCH_2CH_2OH$) which form a negative, positive, and hydrophilic surfaces, respectively. Then the substrates were incubated in PS I solution and it was found that 65% of the area was covered with PS I when treated with mercaptoacetic acid. The negatively charged end groups attract and orient PS I RCs on the substrate. Previous studies have shown that the polar regions (both ends) of the PS I are positively charged [56]. These regions serve as the docking sites for ferredoxin and plastocyanin, the natural electron acceptor and donor, respectively, for PS I. On the other hand, very little PS I coverage was found (5.0%) on 2-dimethylaminoethanethiol treated Au surface terminated with positively charged end groups [56]. When treated with 2-mercaptoethanol, 70% of the area was covered with PS I. The treatment with 2-mercaptoethanol terminates the surface with end groups that form hydrogen bonds with PS I arrays.

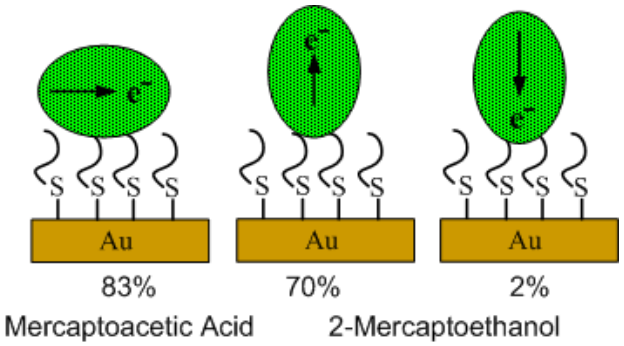

Figure 4.4: Orientation of PS I molecules after treating the gate with Marcaptoacetic acid and 2-Marcaptoethanol.

In addition, PS I can be selectively oriented by the modification of a surface with the specific organosulfur compounds/thiols [56]. For mercaptoacetic acid, 83% of the electron transport vectors were found parallel to the surface, whereas with 2-mercaptoethanol 70% were oriented perpendicularly in the "up" position with P700 facing the Au surface and only 2% were in the "down" position (Figure 4.4). No preferential orientation was observed with 2-dimethylaminoethanethiol.

4.4.1.2 Experimental Setup

The surface of the AlGaN/GaN HEMT was treated with 2-mercaptoethanol to functionalize the PS I RCs. After waiting for 30 seconds, the die was immersed in PS I solution and was kept in refrigerator for 24 hours. The DC current-voltage (I-V) characteristics have been measured by a Signatone Checkmate DC probe station and a Keithley 2400 source meter. The measurements have been performed in floating gate configuration, i.e., without any applied gate bias. The test conditions were kept identical before and after the immobilization of RCs and as well as in the dark and in the light environments. A Labview program was developed to measure the current-voltage characteristics in all conditions. The floating gate test set-up is shown in Figure 4.5.

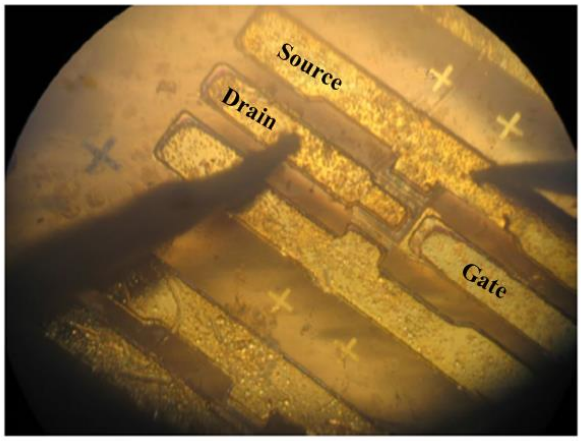

Figure 4.5: Test setup used for the measurement purpose using Signatone Checkmate probe station. The devices are configured in floating gate configuration, as can be seen above.

4.4.1.3 Test Results and Interpretation

The measured I-V characteristics of the HEMT device are shown in Figure 4.6. The drain current before and after the immobilization of the PS I RCs is measured in both light and dark environments. Figure 4.6b shows drain current after immobilizing PS I RCs before and after illumination. The net change in the light and the dark characteristics of the HEMT due to the immobilization of PS I RCs on the gate is also shown in Figure 4.6b. The charge separation mechanism due to light and the resultant changes in the drain current are explained in Figure 4.7.

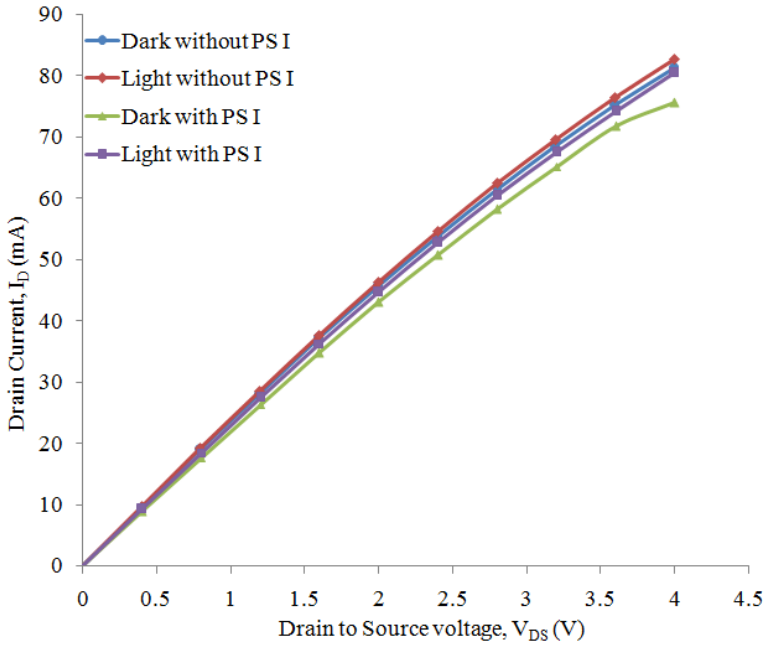

(a)

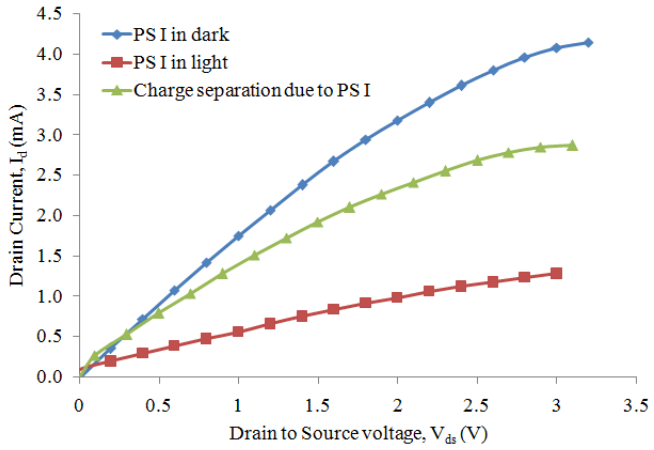

(b)

Figure 4.6: (a) Measured I-V characteristics before and after the immobilization of PS I in light and dark environment, (b) Changes in the I-V characteristics of the device as a result of PS I immobilization and charge separation in PS I RC under illumination.

The orientation for most of the reaction centers on the 2-mercaptoethanol treated surface can be determined by noticing the changes in the current directions due to PS I immobilization. As reported in [56], 70-80% of PS I molecules on 2-mercaptoethanol-modified Au surfaces are oriented primarily with the electron acceptor side (F_{AB}) up and the donor side (P700) down (adjacent to the 2-mercaptoethanol-modified gate surface).

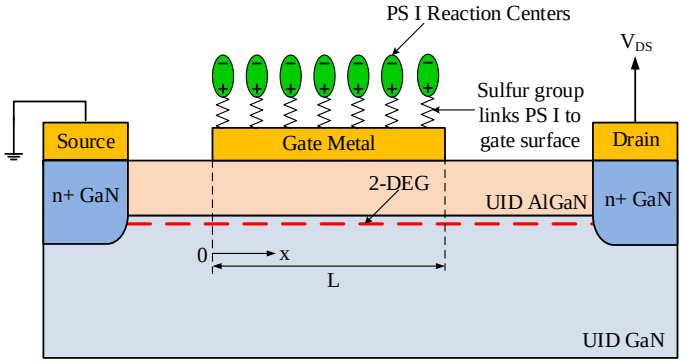

(a)

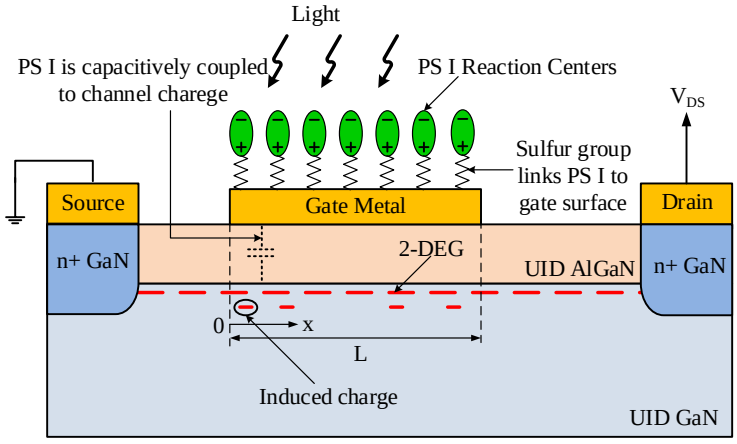

(b)

Figure 4.7: Conceptual illustration of the effect of the dipolar nature of the RCs on the threshold voltage of the HEMT device with immobilized PS I in (a) dark and (b) under light environment.

Under illumination, the electric potential on the oxidizing side (P700) of PS I results in a positive voltage following electron release, whereas in the dark the potential is negative with respect to the substrate [58]. Therefore, each of the reactions centers in the dark can be modeled as a dipole with negative terminal near the substrate which in effect increases the threshold voltage of the HEMT and reduces the current (Figure 4.7a). The current for PS I in dark is negative. Figure 4.6b is plotted by taking the magnitudes of all three currents.

Under illumination, the current should have been reversed completely because of the inversion of dipole polarities (Figure 4.7b). However, during measurement a percentage of the reaction centers become denatured due to the oxygen in the atmosphere, and refrains the current from completely reversing its direction. Figure 4.6a shows the net current of the HEMT in the presence of PS I under illumination. Therefore, the difference in the light and the dark currents due to PS I provides a measure of the current for charge separation across the photoactive reaction centers. The resulting current due to photon induced redox process in the reaction centers is also shown in Figure 4.6b.

4.4.2 Human Monokine Induced Interferron Gamma

Although, organ and tissue transplantation is an increasingly important patient treatment option in a number of disease conditions (for example, kidney, liver, skin, heart, etc.), the rate of allograft rejection episodes is still quite high, occurring in approximately 20% of the recipients [59]. Thus, rejection of transplanted organs or tissues constitutes impedance to the successful long-term treatment of some of the disease conditions. Chemokines are a family of cytokines that have been shown to be crucial mediators of immune reactions leading to transplant or allograft rejection [59]. Specifically, evidence from various studies have clearly shown monokine induced by interferon-gamma (MIG/CXCL9) as playing a central role among the chemokine proteins implicated in rejection of heart, skin and kidney tissue allografts. MIG, a member of the CXC subfamily of chemokines is an inflammatory chemokine that play an

important role in cell activation, and is produced during T-cell-mediated responses to inflammation including allograft rejection episodes) [60,61]. Consequently, MIG is investigated as a target immune response biomarker in transplant applications [60, 62, 63]. The range of MIG concentration in normal and pathophysiological disease states (including allograft rejection episodes) in humans is ≈ 0.2-3 ng/mL and 10-400 ng/mL, respectively [64]. Due to the important role of MIG as a biomarker in transplant rejection, there is a great need to develop biosensor technology platforms to sensitively detect MIG for early monitoring of possible transplant rejection.

4.4.2.1 Functionalization of the BioFET

The sensing gate channel of the HEMTs have gold contact deposition, which is suitable for creating self-assembled monolayers (SAMs) to immobilize the biomolecules. The self-assembly method for anchoring of the biorecognition molecules have a number of advantages relative to other approaches, namely, high reproducibility, molecular level control, vicinity from the surface, allowing direct electron/charge transfer[65]. Dithiobis(succinimidyl propionate) or DSP is a water insoluble, homobifunctional N-hydroxysuccinimide (NHS) ester that can form a self-assembled monolayer on a gold surface due to its disulphide group [66]. The NHS group has primary amines as principle targets; consequently it has found applications for the immobilization of biomolecular species (proteins, etc) containing primary amines to gold surface [67]. The bisymmetrical DSP links to ε-amine groups on the α-amine position of N-terminal amino acids. The succinimidyl ester of DSP is an ideal leaving group to electron donating primary amines. Attack occurs at the electron deficient carbon of the ester on DSP by a primary amine to create an amide bond in suitable pH range for the covalent immobilization of the protein on the gold surface. The great advantage of building DSP SAMs in comparison to conventional methods [68, 69] is the elimination of the chemical activation step in the covalent attachment of biomolecules containing primary amines to create an amide bond (Figure 4.8).

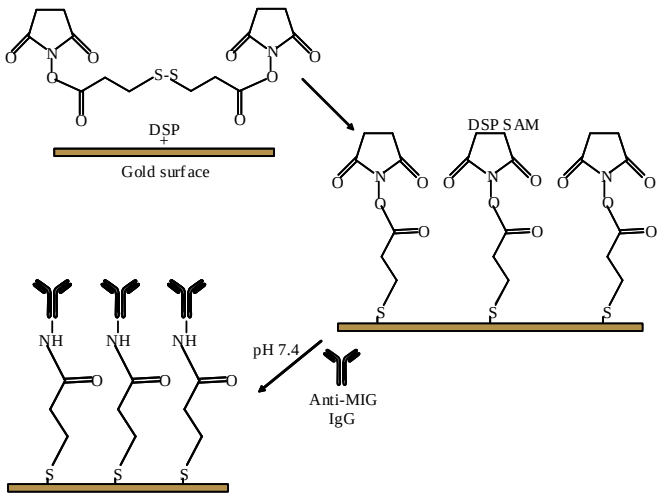

Figure 4.8: Schematic illustrating the formation of reactive DSP SAM on HEMT gold gate for covalent immobilization of anti-MIG monoclonal IgG.

The vicinity of short DSP SAMs from the electrode surface has been used previously to obtain direct electron transfer from redox copper centers [70]; DSP has spacer arm length of 12.0 Å or 8 atoms [71]. The short height of the SAM and the elimination of additional layers of chemical activating groups are advantageous for FET sensing architectures where proximity of the binding antibody-antigen pairs to the sensing gate surface is crucial for sensitive detection of the binding event.

4.4.2.2 Experimental Setup

Prior to any experimental work, the device was properly cleaned with acetone and ethanol and dried in nitrogen flow. To create the SAM layer, the gold gate region was exposed to 1 mM solution of DSP for two hours at room temperature. To remove the weakly absorbed DSP, the device was again washed away using acetone. The reactive SAM layer created covalently binds the anti-MIG monoclonal IgG molecules through their primary amine groups. To achieve immobilization, the gate was exposed to 25µL anti-MIG 1gG in phosphate buffered saline (PBS) at 40C for 24 hours. Rinsing the device with Tween 20 solution

in PBS washes away the weakly bound anti-MIG. The change in the drain current due to the immobilization of the anti-MIG was measured. The resulting molecular affinity interface IgG receptors are then used for the binding and detection of the MIG. To accomplish this, the biofunctionalized gate was exposed to 20 ng/mL human MIG in PBS (150 mM) and the change in drain current due to the anti-MIG/MIG binding interaction was measured. The volume applied is 25µL. Similar measurement was also carried out separately for 50 ng/mL MIG concentration. Before repeating the experiment with the same device, it was properly cleaned to eliminate any trace of analyte from the previous experiments. The step by step procedure is shown in Figure 4.9.

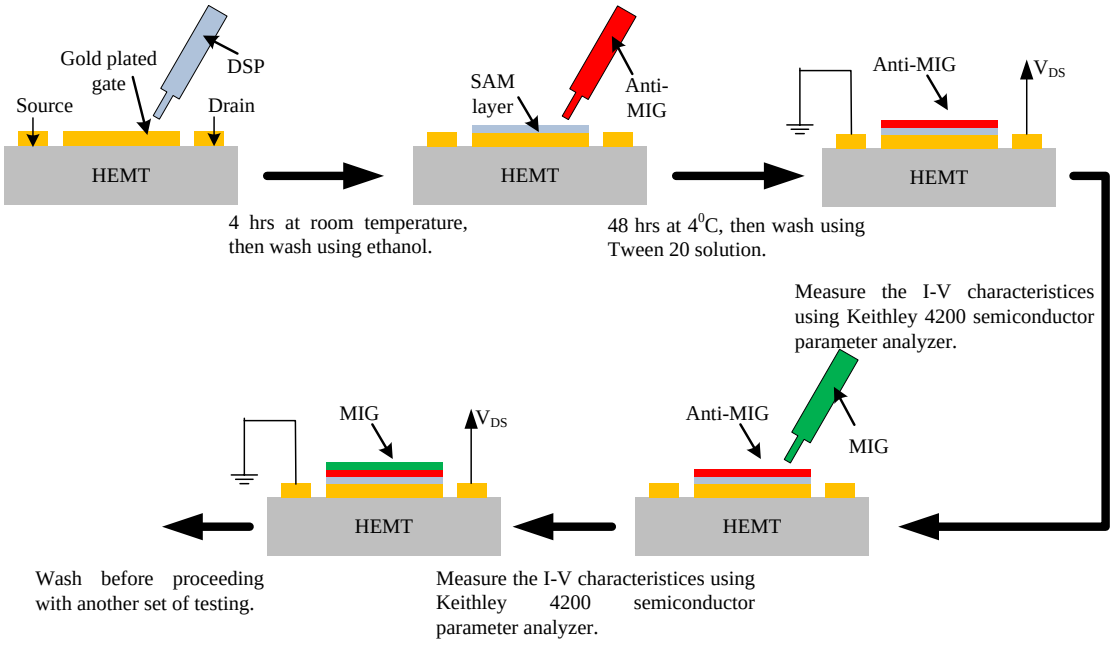

Figure 4.9: Step by step procedure for testing using GaN/AlGaN biosensor.

4.4.2.3 Test Results and Interpretation

After the formation of SAM layer, the device current was a little lower compared to that of the clean device. This slight decrease in current may be due to the change in the gate surface after the SAM layer was created. However, exposure to anti-MIG IgG changed the drain current significantly. The anti-MIG molecules immobilized on the gate surface of the device impart specific biorecognition properties to the HEMT BioFET sensor. As it has been reported that antigens elicit antibodies of opposite charge and that the antigen-binding sites dominate the interface properties of IgG antibodies [72, 73], it is assumed that the positive polarity of the anti-MIG IgG molecules lies adjacent to the gate surface.

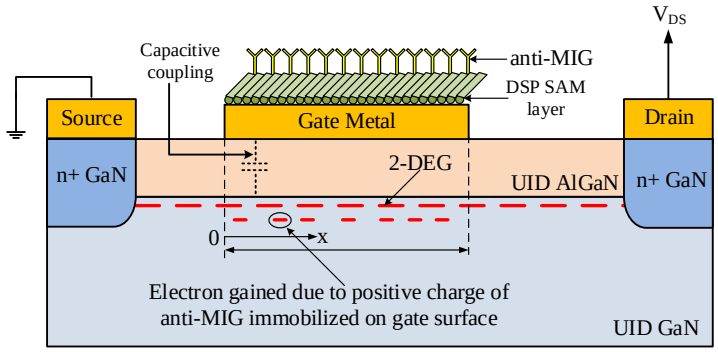

Figure 4.10: Increase in drain current after anti-MIG immobilization on gate.

Each positive charge on the gate surface induces a negative charge in the 2DEG due to capacitive coupling and thus results in an increase in the gate current. This is schematically shown in Figure 4.10 and is confirmed by the measured data in Figure 4.12.

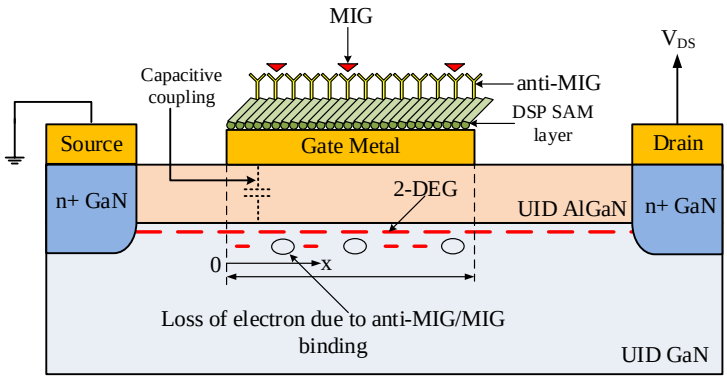

Figure 4.11: Decrease in drain current due to loss of electron after MIG/anti-MIG binding.

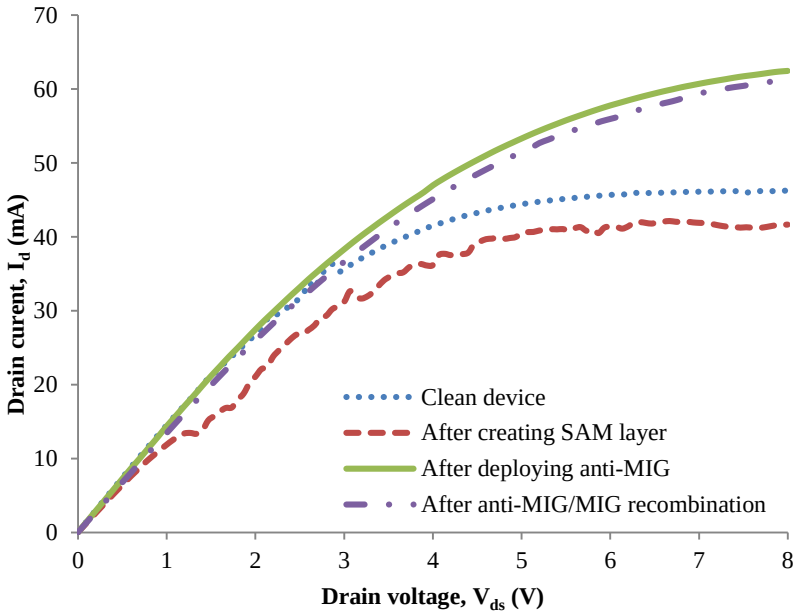

Figure 4.12: Measurement of drain current for clean device, after anti-MIG immobilization and after MIG exposure. Current reduces by 1.9mA due to recombination of anti-MIG and MIG.

The recombinant human MIG exposed to the device sensing gate binds specifically with the previously immobilized anti-MIG IgG molecules. The corresponding changes in the net charge of the MIG/anti-MIG complex modulate the electrical properties of the HEMT FET sensing channel. These results in loss of the electron gained in the previous anti-MIG immobilization and cause a decrease in the drain current. As already indicated above, this is shown in Figure 4.11 and is confirmed by the measured data in Figure 4.12. The experimental results confirm the sensitive detection of the MIG by the anti-MIG monoclonal antibody.

Experiments were carried out using various concentrations of MIG, ranging from 5 ng/mL to 500 ng/mL. It was observed that at low concentrations range the increasing MIG concentration decreased the differential current due to anti-MIG/MIG recombination. As the anti-MIG concentration was held constant, increasing MIG concentration results in a gradual increase in the drain current after immobilization due to the presence of the positive charge on the MIG. As a result, the differential current before and after the immobilization of MIG is gradually decreased as shown in Figure 4.13. Figure 4.14 represents the reproducibility of the result with three sets of test data at 5ng/mL concentration of MIG that fall within the standard error bars.

As MIG concentration was further increased, the positively charged MIG dominates the net charge at the gate. Due to the dominating positive gate charges, electrons are attracted to the channel resulting in the increase in the drain current. Eventually the current after immobilization of the MIG becomes greater than the current prior to the immobilization. As a result, the differential current increases in the negative direction, which is confirmed by Figure 4.13.

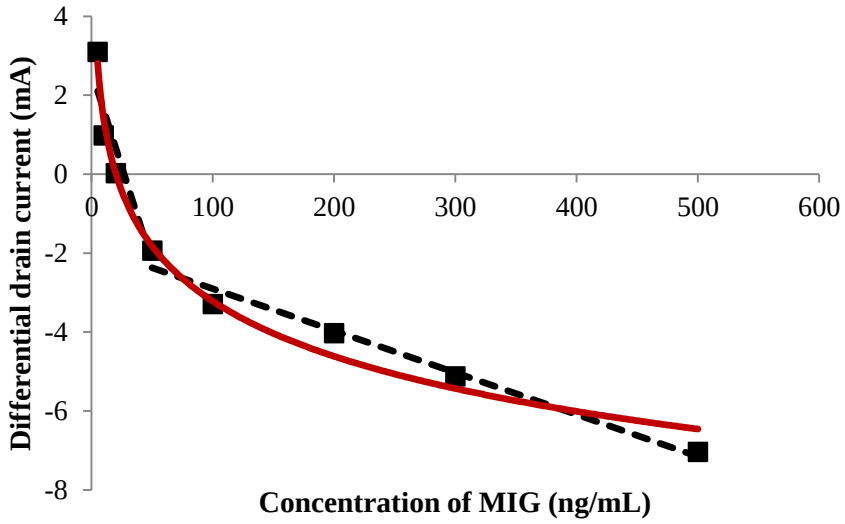

Figure 4.13: Decrease in differential drain current with increase in MIG concentration. V_{ds} is kept fixed at 2 V.

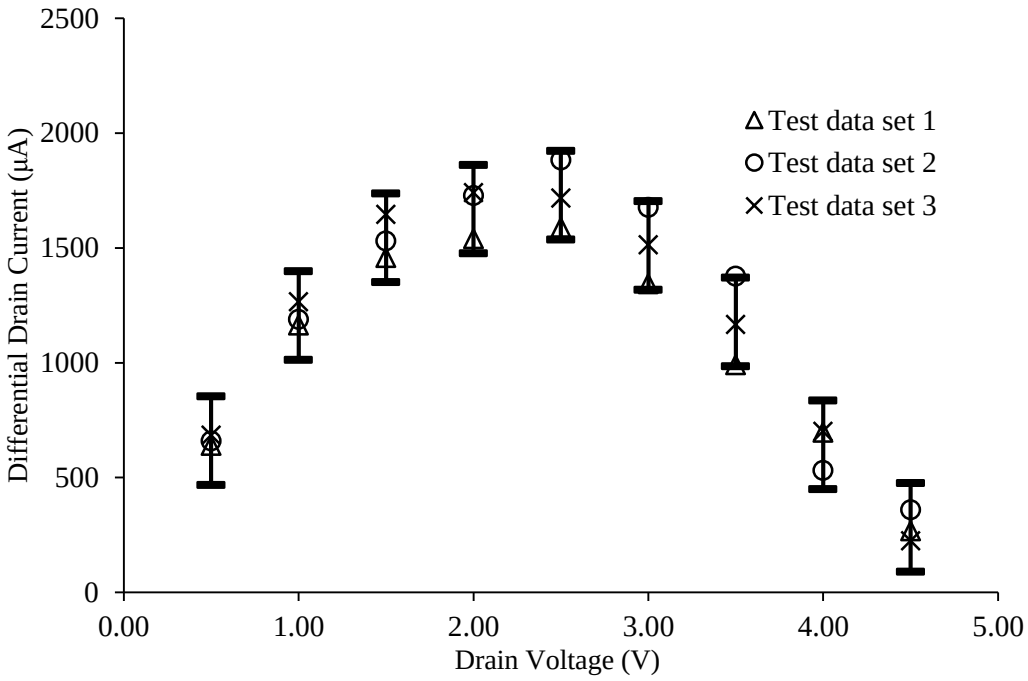

Figure 4.13: Standard error bars demonstrating the reproducibility of the results. The concentration of MIG was maintained at 5ng/mL.

4.5 Conclusion

Using the same device, a novel way for detecting two different kinds of biomolecules is demonstrated, which promises the potential of detecting multiple biomolecule in a single chip. As such, the sensor can be further developed for point of care applications for the detection of biomarkers of complex diseases such as different types of cancers, where detecting only one or two biomarkers may give ambiguous results. The device can be integrated with microfluidic channels to control the flow of target analyte to the area of interest and with other signal processing and transmission circuitry to have a lab on a chip.

In addition, the results reported here is the first for the detection of native recombinant human MIG in physiologically relevant buffer environment (150 mM PBS). This shows the potential of the devices for use in the detection of biomarkers in an ionic strength environment corresponding to that present in human blood. This possibility will eliminate the need for the extra steps required to extract the target biomarkers and prepare diluted solution before detection.

Chapter 5
Charge Control Model of HEMT

5.1 Introduction

This chapter focuses on the development of a physics based analytical model of AlGaN/GaN HEMT. The development of 2D electron gas (2DEG) in HEMT structure is investigated in details. Both spontaneous and piezoelectric effects of polarization in channel charge are considered. A quasi-triangular quantum well is considered in the heterojunction. The sheet carrier density of the 2DEG is expressed via a non-linear equation. The non-linear equation of charge is simplified based on realistic approximation and the current voltage relationship of the HEMT device is developed. The effect of drift velocity and electric field is also included via an empirical model.

5.2 Development of 2D Electron Gas in AlGaN/GaN HEMT

The crystalline structure of GaN can be both Zinc blende and Wurtzite (Figure 5.1). It is normally grown on the Ga-face, along the c-axis.

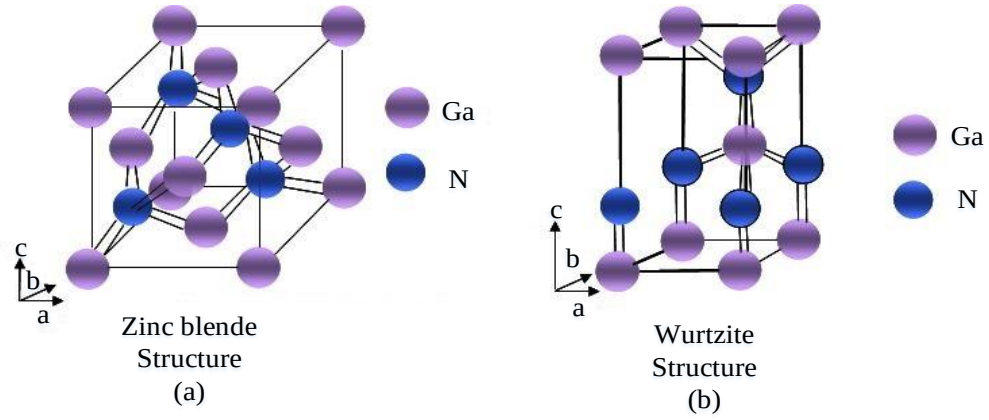

Figure 5.1: Crystalline structure of GaN.

Because of the noncentrosymmetry in its crystalline structure, GaN exhibits a substantial spontaneous electrical polarization (P_{sp}) perpendicular to the hexagonal plane, and in the direction down into the Ga-face surface, as shown in Figure 5.2. When AlGaN is grown on GaN, larger electrical polarization results in the same direction. Moreover, since AlGaN has a smaller lattice constant than GaN, the two-dimensional tension at the interface induces a piezoelectric polarization component (P_{pe}) which adds to the spontaneous polarization [53].

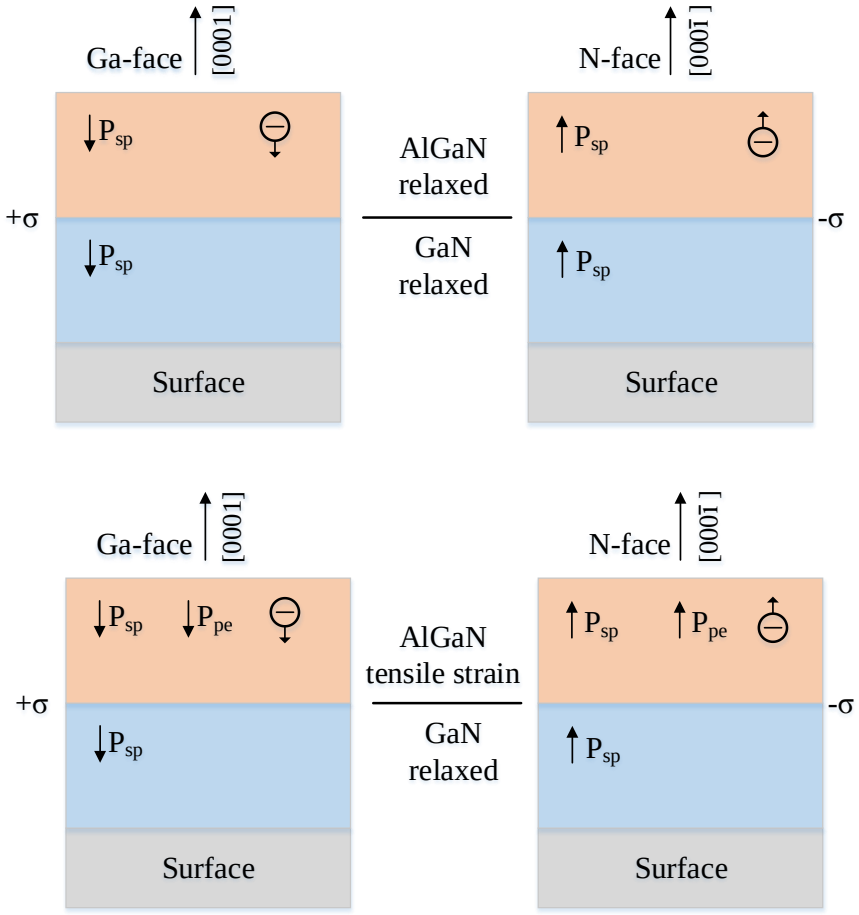

Figure 5.2: Polarization properties of AlGaN and GaN materials.

The total electrical polarization (P_t) between the pseudomorphic AlGaN top barrier layer and the GaN channel layer is obtained by the algebraic sum of individual components as given by equation 5.1.

$$P_t = P_{sp}(AlGaN) - P_{sp}(GaN) + P_{pe}(AlGaN) \quad (5.1)$$

A positive sheet charge density (Q) appears due to the net polarization effect, which causes an accumulation of electrons at the interface and thus forms the 2-DEG (Figure 5.3). Therefore, even without any intentional doping in the AlGaN layer, a high charge density channel is formed at the heterointerface.

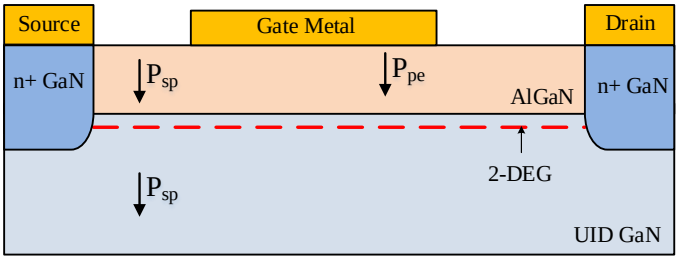

Figure 5.3: Formation of 2DEG at AlGaN/GaN hetero-interface due to spontaneous and piezoelectric polarization.

Especially in wurtzite AlGaN/GaN based transistor structures; the piezoelectric polarization of the strained top layer is more than five times larger as compared to that of AlGaAs/GaAs structures, leading to a significant increase of the sheet carrier concentration at the interface [74].

The amount of charge density due to spontaneous charge density in case of AlGaN is 0.055 C/m^2 [75]. The Amount of charge density because of piezoelectric polarization is given by

$$Q_{pe} = 2\frac{a_{GaN}-a_{AlGaN}}{a_{AlGaN}}\left(e_{31} - e_{33}\frac{C_{13}}{C_{33}}\right) \quad (5.2)$$

where, a is the lattice constant of the material, e is the piezoelectric co-efficient and C is the relevant elastic constant.

5.3 Non-linear Charge Control Model

The first model to predict the charge concentration at the heterojunction of a HEMT device was proposed by D. Delagebeaudeuf and N. T. Linh [76]. Based on AlGaAs/GaAs HEMT, they proposed that the charge concentration at the 2DEG is given by

$$Q_s = qn_s = \frac{\epsilon_2}{d}\left(V_g - \frac{E_F}{q} - V_{off}\right)$$

where, Q_s is the channel charge, n_s is the sheet carrier density, ϵ_2 is the permittivity of the higher bandgap material, d is the effective distance between the Schottky gate and 2DEG, E_F is the Fermi energy at the interface, V_g is the applied gate voltage, and V_{off} is the voltage that annihilates the 2DEG and is given by

$$V_{off} = \varphi_B - \frac{\Delta E_c}{q} - \frac{qN_2}{2\epsilon_2}(d-e)^2 - \frac{d}{\epsilon_2}Q_i \quad (5.3)$$

where, φ_B is the Schottky barrier height, ΔE_C is the conduction band offset at the hetero-interface, e is the thickness of the spacer layer, Q_i is the interface state charge.

Now, E_F is dependent on V_g and results in a nonlinear equation for n_s, and in case of a triangular potential well, the relationship between E_F and n_s is given by [77]

$$E_F = E_{F0} + \gamma {n_s}^{\frac{2}{3}}$$

where, E_{F0} is equilibrium Fermi level and γ is a constant linking the 2DEG carrier density with the longitudinal quantized energy. This approximation is valid as long as the device is not operated in the deep subthreshold region.

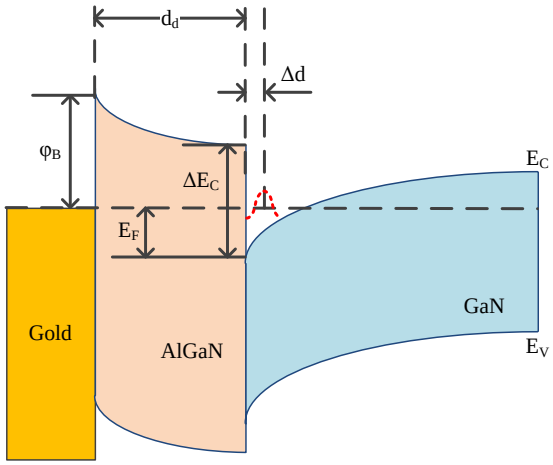

Figure 5.4: Energy band diagram of AlGaN/GaN HEMT.

For AlGaN/GaN HEMT devices, equation 5.3 can be modified depending on the Energy band diagram as shown in Figure 5.4 as follows [78]:

$$n_s(x) = \frac{Q_s}{q} = \frac{q\epsilon_2}{q^2 d + \epsilon_2 a}\left(V_g - V(x) - V_{th}\right) \tag{5.4}$$

where, a is the quantum well shape factor, $V(x)$ is the channel potential at x, V_{th} is the threshold voltage, and $d = d_d + d_r + \Delta d$, where d_d is the thickness of AlGaN layer, d_r is the roughness of gate metal and Δd is the offset of the 2-DEG from the hetero-interface.

The threshold voltage V_{th} is given by

$$V_{th} = V_{off} + E_F$$

For AlGaN/GaN HEMT, V_{off} is defined by

$$V_{off} = \varphi_B - \frac{\Delta E_c}{q} - \frac{qN_2}{2\epsilon_2} d^2$$

Using equation 5.4, the equation for sheet carrier density can be rewritten as

$$n_s(x) = \frac{q\epsilon_2}{q^2 d + \epsilon_2 a} \left(V_g - V(x) - \varphi_B + \frac{\Delta E_c}{q} + \frac{qN_2}{2\epsilon_2} d^2 - E_{F0} - \gamma n_s^{\frac{2}{3}} \right) \qquad (5.5)$$

5.4 Current Voltage Characteristics

The drain current is given by [79],

$$I_d = q n_s Z v(x) \qquad (5.6)$$

where, Z is the gate width and $v(x)$ is the electron drift velocity. The relationship between the drift velocity and the electric field used by in this work is expressed as [29],

$$v(x) = \frac{v_s E(x)}{\sqrt{E^2(x) + \left(\frac{v_s}{\mu_0}\right)^2}} \qquad (5.7)$$

where, v_s is the saturation drift velocity and μ_0 is the low-field mobility.

Using equations 5.5 to 5.7, the drain current equation can be written as

$$I_d = \frac{q^2 \epsilon_2}{q^2 d + \epsilon_2 a} \left(V_g - V(x) - \varphi_B + \frac{\Delta E_c}{q} + \frac{qN_2}{2\epsilon_2} d^2 - E_{F0} - \gamma n_s^{\frac{2}{3}} \right) Z \frac{v_s E(x)}{\sqrt{E^2(x) + \left(\frac{v_s}{\mu_0}\right)^2}} \qquad (5.8)$$

5.4.1 Drain Current Before Saturation

From the boundary conditions, it is obvious that $V(x) = 0$ at $x = 0$, and $V(x) = V_{ds}$ at $x = L$, where L is the length of the HEMT.

From equation 5.8,

$$I_{d,0} = \frac{q^2 \in_2}{q^2 d + \in_2 a}\left(V_g - \varphi_B + \frac{\Delta E_c}{q} + \frac{qN_2}{2\epsilon_2}d^2 - E_{F0} - \gamma n_s^{\frac{2}{3}}\right) Z \frac{v_s E(x)}{\sqrt{E^2(x) + \left(\frac{v_s}{\mu_0}\right)^2}}$$

$$I_{d,L} = \frac{q^2 \in_2}{q^2 d + \in_2 a}\left(V_g - V_{ds} - \varphi_B + \frac{\Delta E_c}{q} + \frac{qN_2}{2\epsilon_2}d^2 - E_{F0} - \gamma n_s^{\frac{2}{3}}\right) Z \frac{v_s E(x)}{\sqrt{E^2(x) + \left(\frac{v_s}{\mu_0}\right)^2}}$$

From equation 5.8,

$$I_d = K_1\left(V_g - V(x) - K_2 - \gamma n_s^{\frac{2}{3}}\right) Z \frac{v_s E(x)}{\sqrt{E^2(x) + \beta}}$$

where, $K_1 = \frac{q^2 \in_2}{q^2 d + \in_2 a}$ and $K_2 = \varphi_B - \frac{\Delta E_c}{q} - \frac{qN_2}{2\epsilon_2}d^2 + E_{F0}$, and $\beta^2 = \left(\frac{v_s}{\mu_0}\right)^2$

So,

$$\frac{\beta^2}{E^2(x)} = \frac{K_1\left(V_g - V(x) - K_2 - \gamma n_s^{\frac{2}{3}}\right) Z v_s}{I_d} - 1$$

Since $E(x) = -\frac{dV(x)}{x}$,

$$-\beta dx = \left\{\frac{K_1\left(V_g - V(x) - K_2 - \gamma n_s^{\frac{2}{3}}\right) Z v_s}{I_d} - 1\right\}^{1/2} dV(x)$$

Or,

$$dV(x) = -\frac{\beta}{\left(\frac{G(x)}{I_d}-1\right)^{1/2}}dx \qquad (5.9)$$

where, $G(x) = K_1\left(V_g - V(x) - K_2 - \gamma n_s^{\frac{2}{3}}(x)\right)Zv_s$.

By integrating equation 5.9 from $x = 0$ to $x = L$, the drain current equation before saturation is obtained using the boundary conditions.

5.4.2 Drain Current After Saturation

Saturation is achieved when channel conductance g_m becomes zero.

$$g_m = \frac{\partial I_d}{\partial V_{ds}} = 0$$

Because of the current continuity at the onset of saturation,

$$I_{d,sat} = \frac{q^2\epsilon_2}{q^2 d+\epsilon_2 a}\left(V_g - V_{ds} - \varphi_B + \frac{\Delta E_c}{q} + \frac{qN_2}{2\epsilon_2}d^2 - E_{F0} - \gamma n_s^{\frac{2}{3}}\right)Z\frac{v_s E_{sat}}{\sqrt{E_{sat}^2+\left(\frac{v_s}{\mu_0}\right)^2}} \qquad (5.10)$$

where, $E_{sat} = -\frac{V_{sat}}{L_{sat}}$.

To find out V_{sat} and L_{sat}, two dimensional Poisson's equation in the pinch-off region can be solved which results in [77]

$$V_d - V_{sat} = \frac{2E_s d_s}{\pi}sinh\left[\frac{L-L_{sat}}{2d_s}\right]$$

where,

$$d_s = d\left\{1 + \gamma\left(\frac{\epsilon_2}{qd}\right)^{2/3}\left(V_g - V_{th} - V_{sat}\right)^{-1/3}\right\}$$

5.5 Comparison of Measurement and Simulation Results

The current voltage characteristics of test devices are obtained by Keithley 4200 semiconductor parameter analyzer and Signatone DC probe station. The transfer characteristics is obtained by keeping the drain to source voltage constant. Figure 5.5 shows the comparison of measured and simulated $I_d - V_{gs}$ curve at V_{ds} = 5 V. The threshold voltage of the HEMT device is observed to be -4.56 V.

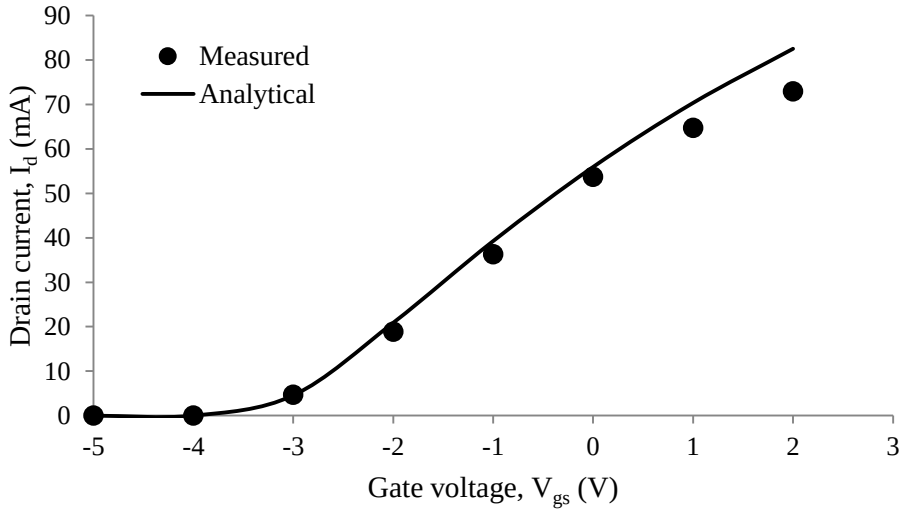

Figure 5.5: Measured and simulated transfer characteristics (I_d-V_{gs}) of the AlGaN/GaN HEMT device. V_{ds} is kept fixed at 5V.

The output characteristics is obtained at varying gate voltage by keeping V_{gs} constant a particular bias and varying V_{ds} from 0V to 5V. The drain current before saturation and after saturation are calculated using equations 5.9 and 5.10. It is observed that the model overestimates the drain current at higher voltages, since a constant resistant throughout the channel is considered.

The output characteristics curves are measured for gate voltage of -2V to +2V by step increment. The measured and simulated $I_d - V_{ds}$ curve is shown in Figure 5.6. For low values of voltage, the simulated curves match the measured output characteristics. But for higher voltages, some discrepancy is observed since the as the secondary effects of the channel saturation such as channel length modulation become prominent, which are ignored in the proposed model for the sake of simplicity.

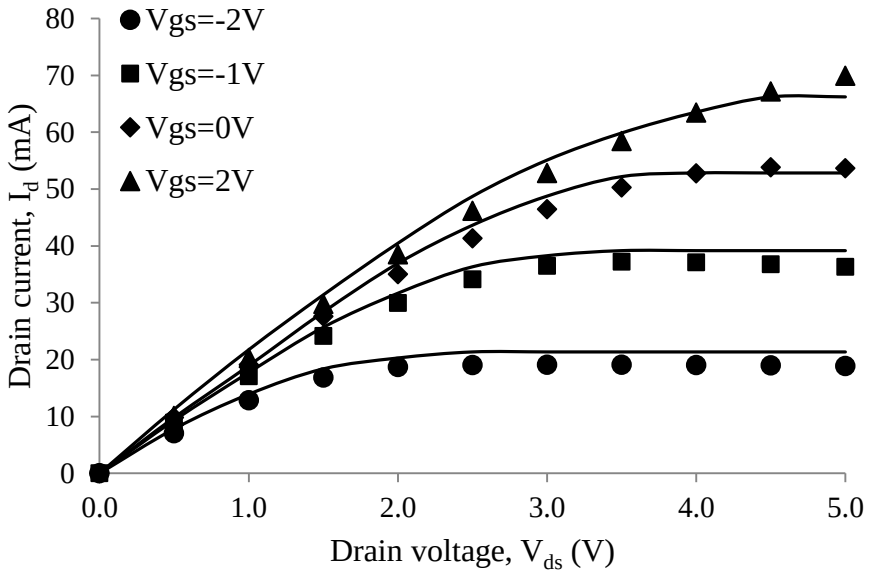

Figure 5.6: Measured and simulated output characteristics (I_d-V_{ds}) of HEMT device. V_{gs} is varied from -2V to +2V. V_{ds} is varied from 0V to 5V

Chapter 6

Floating Gate Model for BioFET

6.1 Introduction

This chapter focuses on the development of a floating gate model suitable for predicting the behavior of biosensor platform. The nonlinear charge control model for evaluation of the drain current as discussed in the previous chapter depends on the applied gate voltage. But in case of biosensor, an applied gate voltage will nullify any effect of the charged biomolecules immobilized on the gate surface. As such, a model is required that predicts the modulation of the channel charge in response of the immobilized gate charge instead of applied gate voltage.

This chapter explains the mechanism of how the charged biomolecules modulate the channel charge underneath the gate and modifies the analytical model developed in the previous chapter into a floating gate model.

6.2 Charge Coupling Through Gate Capacitance

Target biomolecules are immobilized on the gate by functionalization of the HEMT sensor. Once immobilized, the charged biomolecules are linked to the channel charge via capacitive coupling method. A positive charge on the gate will induce more electrons in the 2DEG below and result in the increase in the drain current. A negative charge on the gate on the other hand will repel electrons from the 2DEG. The loss of electron in the channel will be reflected via a reduction in the drain current. Since no external voltage is applied, the configuration is considered to be a floating gate condition. The capacitive coupling of the charge molecules will change the electric field distribution and as such will be reflected as floating gate voltage.

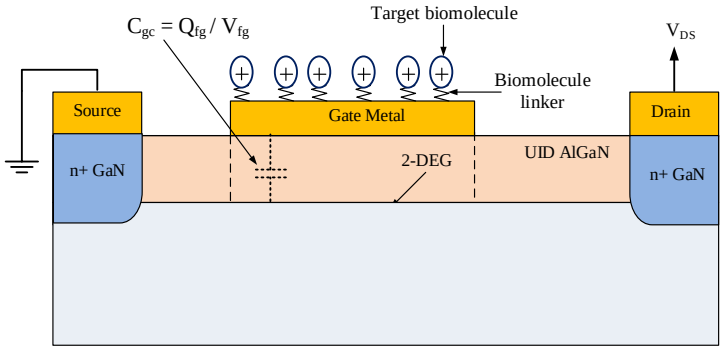

Figure 6.1: Schematic of floating gate AlGaN/GaN HEMT with gold contacts at gate, drain and source region. Target biomolecules are adsorbed onto the gold contacts of the gate and become capacitively coupled to the channel underneath.

The relationship between the floating gate charge Q_{fg}, the reflected voltage at the floating gate V_{fg}, and the gate-to-channel capacitance C_{gc} is simply given by

$$Q_{fg} = C_{gc}V_{fg} \tag{6.1}$$

This gate charge will affect the electrostatic distribution in the channel and modify the sheet carrier density according to the following equations:

$$n_s = \frac{Q_s}{q} = \frac{\epsilon_2}{d}\left(\varphi_b + \frac{E_F}{q} - \frac{\Delta E_c}{q} + V_c(x)\right) \tag{6.2}$$

$$n_s + \Delta n = \frac{\epsilon_2}{d}\left(\varphi_b + \frac{E_F}{q} - \frac{\Delta E_c}{q} + V_c(x) - \frac{\Delta d + d_d}{d}V_{fg}\right) \tag{6.3}$$

where, Q_s is the channel charge, Δn is the modified sheet carrier density due to the floating gate voltage, ϵ_2 is the permittivity of AlGaN, φ_b is the Schottky barrier height, E_F is the Fermi energy at the interface relative to the GaN conduction-band-edge, ΔE_C is the conduction band offset at the AlGaN/GaN interface, $V_C(x)$ is the channel potential at x, and $d = d_d + d_r + \Delta d$, where d_d is the thickness of AlGaN layer, d_r is the roughness of gate metal and Δd is the offset of the 2-DEG from the heterointerface.

6.3 Current Voltage Characteristics

The sheet carrier density from equations 6.2 and 6.3 can be used to calculate the drain current before and after the immobilization of the biomolecules via equations 6.4 and 6.5 as shown below,

$$I_D = qn_sZv(x) \tag{6.4}$$

$$I_D + \Delta I_D = q(n_s + \Delta n)Zv(x) \tag{6.5}$$

where, the drift velocity is replaced by the velocity-electric field empirical relationship of the previous chapter and we get

$$I_D = q\frac{\epsilon_2}{d}\left(\varphi_b + \frac{E_F}{q} - \frac{\Delta E_c}{q} + V_c(x)\right)Z\frac{v_sE(x)}{\sqrt{E^2(x)+\left(\frac{v_s}{\mu_0}\right)^2}} \tag{6.6}$$

$$I_D + \Delta I_D = q\frac{\epsilon_2}{d}\left(\varphi_b + \frac{E_F}{q} - \frac{\Delta E_c}{q} + V_c(x) - \frac{\Delta d+d_d}{d}V_{fg}\right)Z\frac{v_sE(x)}{\sqrt{E^2(x)+\left(\frac{v_s}{\mu_0}\right)^2}} \tag{6.7}$$

where, v_s is the saturation velocity of electrons in GaN, μ_0 is the low-field mobility of electron in the 2-DEG.

The mechanism of change in drain current before and after the immobilization of biomolecules is shown in Figure 6.2.

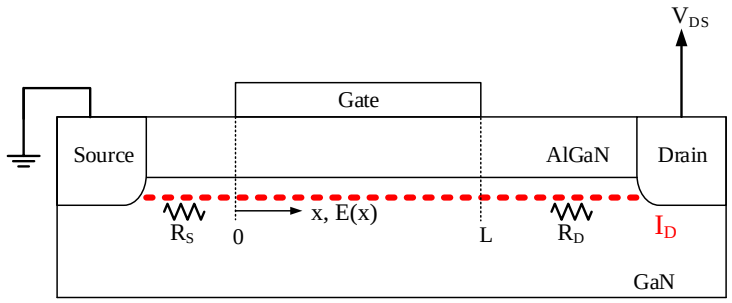

(a)

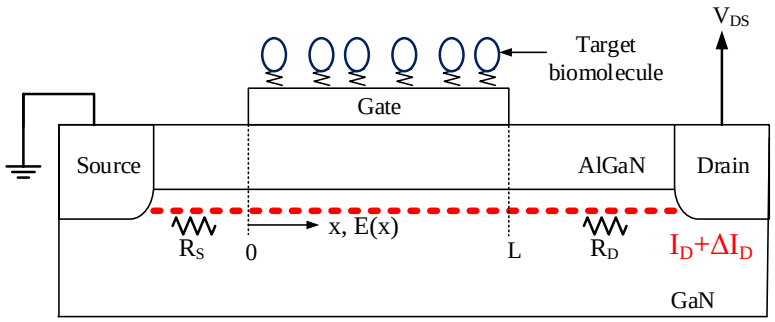

(b)

Figure 6.2: Changes in the drain current due to biomolecule immobilization: (a) Current before immobilization of biomolecules, (b) Current after the immobilization of biomolecules.

From equations 6.6 and 6.7, the change in the drain current due to the immobilized biomolecules can be given by

$$\Delta I_D = q\frac{\epsilon_2}{d}\left(-\frac{\Delta d+d_d}{d}V_{fg}\right)Z\frac{\nu_s E(x)}{\sqrt{E^2(x)+\left(\frac{\nu_s}{\mu_0}\right)^2}} \tag{6.8}$$

6.4 Effect of Threshold Voltage Shift

The threshold voltage changes due to the dipoles of the target biomolecules, which can be written as [80, 81]

$$\Delta V_{th} = \frac{\mu_{dip} N_b}{\epsilon} \tag{6.9}$$

where, μ_{dip} and ϵ are the dipole moment and the dielectric permittivity of the biomolecule, respectively, N_b is the surface density of the charged molecules vertically oriented on the gate.

Under floating gate condition, the sheet carrier density, $n_s(x)$ is redefined from equation 5.5 by,

$$n_s(x) + \Delta n_s = \frac{\epsilon_2}{q(d_d+\Delta d)}(-V(x) - V_{th} - \Delta V_{th}) \tag{6.10}$$

where, $V(x)$ is the voltage along the x-direction in the 2-DEG channel due to applied drain bias [9, 10].

$$V_{th} = \varphi_B - \frac{\Delta E_c}{q} - \frac{N d_d}{\epsilon_2} + \frac{E_F}{q} \tag{6.11}$$

where, N is the sheet charge density due to spontaneous and piezoelectric polarizations.

From equations 6.9 to 6.11, the change in sheet carrier density due to shift in threshold voltage can be expressed by

$$\Delta n_s = \frac{\epsilon_2}{q(d_d+\Delta d)}\left(-\frac{\mu_{dip} N_b}{\epsilon}\right) \tag{6.12}$$

As such, the change in the drain current can be given by

$$\Delta I_D = \frac{\epsilon_2}{(d_d+\Delta d)}\left(-\frac{\mu_{dip} N_b}{\epsilon}\right) Z \frac{\nu_s E(x)}{\sqrt{E^2(x)+\left(\frac{\nu_s}{\mu_0}\right)^2}} \tag{6.13}$$

6.5 Comparison of Measurement and Simulation Results

The changes in the drain current before and after the immobilization of the target biomolecules are measured using Keithly 4200 semiconductor parameter analyzer and Signatone Checkmate probe station. The measured test data is compared with the simulation results based on the proposed floating gate model, as shown in Figure 6.3. For low values of drain voltage (upto 2V), the measured data closely follows the simulation data.

It is also observed from test data that as biomolecule concentration at the gate increases, the drain current reaches saturation at a lower reflected gate voltage. It is because increased biomolecule concentration at the gate increases the net charge available at the gate. As a result, the required voltage to reach peak current is decreased. This phenomenon is exhibited in Figure 6.4.

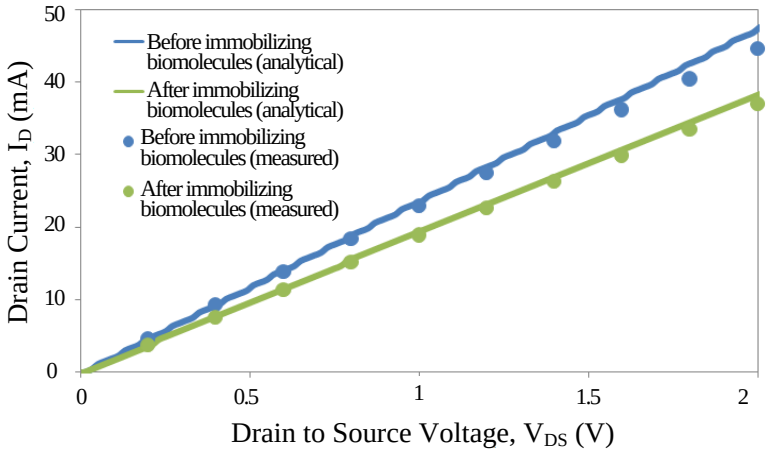

Figure 6.3: Simulated and measured changes in the drain current due to immobilization of target biomolecule.

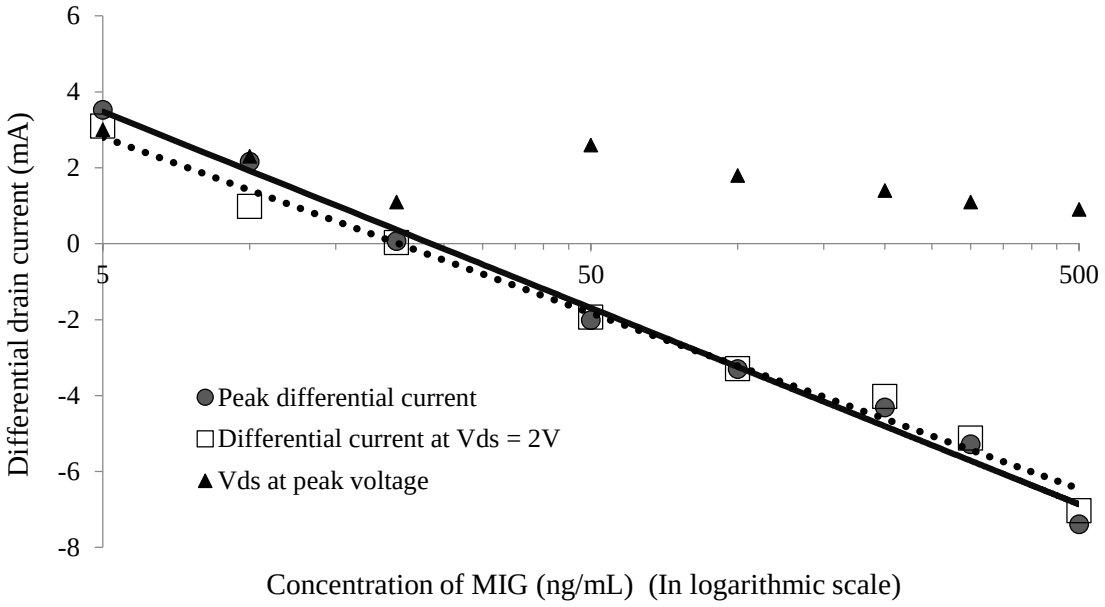

Figure 6.4: Variation in V_{ds} at which peak differential current occurs with the increase in biomolecule concentration. The x axis is shown in logarithmic scale for better comprehension.

Chapter 7

Discussions and Conclusions

6.1 Conclusions

Different biosensor platforms have been investigated in detail in this work. After careful comparison of these biosensor platforms, AlGaN/GaN HEMT based biosensor platform is chosen for the detection of multiple biomolecules. An analytical model considering the effect of polarization which forms a 2DEG in a triangular quantum well is proposed. Based on the physics based analytical model, a floating gate model has been derived to predict the behavior of the AlGaN/GaN HEMT based biosensor platform.

The original contributions, as pointed out by this work are:

- Configuring an AlGaN/GaN HEMT as a bioFET for the first time.
- Detection of multiple target biomolecules using the same platform.
- Measurement of target biomolecule (MIG) in physiologically relevant environment for the first time.
- Improving the existing model of HEMT by including the effect of polarization which creates the channel in AlGaN/GaN HEMT.
- Predicting the behavior of the proposed bioFET by modifying the proposed model in a floating gate configuration.

6.2 Future Works

Compared to Si technology, AlGaN/GaN devices are still at the preliminary stages of their development and fabrication. As such, gate leakage, traps and surface defects are some still hinder the commercialization of high performance wide bandgap GaN devices. But because of their immense prospect, GaN might be the device of the future. As such, a physics-based analytical model to predict the device behavior is of utmost importance. Including the effects of following phenomena would help understand the device behavior more accurately:

- Parasitic parallel conduction for higher gate voltage
- Variation of drain and source resistances with gate voltage and temperature
- Leakage currents
- Trapping effects

In this work, the DC current-voltage characteristics of AlGaN/GaN HEMT have been validated by the measured data. The proposed model is also used to predict the behavior of a biosensor realized in AlGaN/GaN HEMT platform for two different kinds of biomolecules for *in vitro* sensing. The biosensor platform can be improved by investing the following conditions:

- Including the effect of interferers that might be present in relevant physiological condition for *in vivo* sensing.
- Validating the model using other charged biomolecules.
- Developing a lab-on-a-chip platform by transferring the output of the HEMT to the signal processing unit.

References

1. "Biosensors Market (Electrochemical, Optical, Piezoelectric & Thermistor) - Global Industry Analysis, Size, Share, Growth, Trends and Forecast, 2012 – 2018," *Transparency Market Research*, June 2013. Available online at http://www.transparencymarketresearch.com/biosensors-market.html.
2. Dr. R. Thusu, "Strong growth predicted for BioSensors market," *Sensors*, October 2010.
3. H. F. Haque, "Temperature Dependent Analytical Modeling, Simulation and Characterizations of HEMTs in Gallium Nitride Process," *Ph. D. Dissertation*, University of Tennessee, Knoxville.
4. S. A. Eliza, "Modeling of AlGaN/GaN High Electron Mobility Transistor for Sensors and High-Temperature Circuit Applications," *Ph. D. Dissertation*, University of Tennessee, Knoxville.
5. L. C. Clark. Jr., "Oxygen sensing electrode," *Trans. Am. Soc. Artif. Intern. Organs*, vol. 21, pp. 41-48, 1956.
6. G. G. Guilbault, J. G. Montalvo, "Urea-specific enzyme electrode," *J. Am. Chem. Soc*., vol. 91, pp. 2164-2565, 1969.
7. C. L. Cooney, J. C. Weaver, S. R. Tannenbaum, D. V. Faller, A. Shields, M. Jahnke, E. K. Pye, L. Wingard. "Enzyme Engineering," *1st edition*, 1974.
8. K. Mosbach, B. Danielsson, "An enzyme thermistor," *Biochim. Biophys. Acta.*, vol. 364, pp. 140-145, 1974.
9. C. Divis, "Remarks on ethanol oxidation by an "Acetobacter xylinum" microbial electrode," *Annal. Microb. A*, vol. 126, pp. 175-186, 1975.
10. D. W. Lübbers, N. Opitz, "The pCO_2/pO_2 optode: A new probe for measuring pCO_2 and pO_2 of gases and liquids." *Z. Naturforsch. C*, vol. 30. pp. 532-533, 1975.
11. D. W. Lübbers, N. Opitz, "Opticl fluorescence sensors for continuous measurement of chemical concentrations in biological systems," *Sensor. Actuator.*, vol. 4, pp. 641-654, 1983.
12. A. H. Clemens, P. H. Chang, R. W. Myers, "The development of Biostator, a Glucose Controlled Insulin Infusion System (GCIIS)," *Hormone and Metabolic Research*, suppl. 7, pp. 23-33, 1977.
13. M. Shichiri, Y. Yamaski, R. Kawamori, N. Hakai, H. Abe, "Wearable artificial endocrine pancreas with needle-type glucose sensor," *Lancet*, vol. 320, pp. 1129-1131, 1982.
14. B. Liedberg, C. Nylander, I. Lundström, "Surface plasmon resonance for gas detection and biosensing," *Sensor. Actuator.*, vol. 4, pp. 299-304, 1983.
15. A. E.G. Cass, A.E.G., G. Davis, G. D. Francis, H. A. O. Hill, W. J. Aston, I. J. Higgins, E. V. Plotkin, L. D. L. Scott, A. P. F. Turner, "Ferrocene-mediated enzyme electrode for amperometric determination of glucose," *Anal. Chem.*, vol. 56, pp. 667-671, 1984.
16. A. P. F. Turner, "Advances in Biosensors 1," 1991.
17. S. J. Alcock, A. P. F. Turner, "Continuous analyte monitoring to aid clinical practice," *IEEE Engineering in Medicine and Biology*, vol. 13, pp. 319-325, 1994.
18. E. Kress-Rogers, "Handbook of Biosensors and Electronic Noses: Medicine, Food and the Environment," 1996.
19. S. F. White, A. P. F. Turner, "Process Monitoring," *Encyclopedia of Bioprocess Technology*, 1999.

20. M. J. Dennison, A. P. F Turner, "Biosensors for environmental monitoring," *Biotechnol. Adv.*, vol. 13, pp. 1-12, 1995.
21. S. Saini, A. P. F. Turner, "Multi-phase bioelectrochemical sensors," *Trend. Anal. Chem*., vol. 14, pp. 304-310, 1995.
22. M. J. Dennison, J. M. Hall, A. P. F. Turner, "Gas-phase microbiosensor for monitoring phenol vapor at ppb levels," *Anal. Chem*., vol. 67, 3922-3927, 1995.
23. S. J. Alcock, S. F. White, A. P. F. Turner, S. Setford, I. E. Tothill, J. M. Dicks, S. Stephens, J. M. Hall, P. J. Warner, British Patent Application 9416002.5, 1994.
24. S. G. Skuridin, Y. M. Yevdokimov, V. S. Efimov, J. M. Hall, A. P. F. Turner, "A new approach for creating double-stranded DNA biosensors," *Biosensors Bioelectron.*, vol. 11, pp. 903-911, 1996.
25. S. D. Psoma, A. P. F. Turner, "The measurement of glucose using simultaneous fluorescence quenching of two indicators," *Proceedings of the 3rd World Congress on Biosensors*, Oxford, UK, 1994.
26. J. D. Newman, S. F. White, I. E. Tothill, A. P. F. Turner, "Catalytic materials, membranes, and fabrication technologies suitable for the construction of amperometric biosensors," *Anal. Chem.*, vol. 67, pp. 4594-4599, 1995.
27. S. A. Jaffari, A. P. F. Turner, "Novel hexacyanoferrate(III) modified graphite disc electrodes and their application in enzyme electrodes—Part I," *Biosen. Bioelectron.*, vol. 12, pp. 1-7, 9, 1996.
28. W. M. Albers, J. O. Lekkala, L. Jeuken, G. W. Canters, A. P. F. Turner, "Design of novel molecular wires for realizing long-distance electron transfer," *Bioelectrochem. Bioenerg.*, vol. 42, pp. 25-33, 1996.
29. A. V. Melechko, V. I. Merkulov, T. E. McKnight, M. A. Guillorn, K. L. Klein, D. H. Lowndes, and M. L. Simpson, "Vertically aligned carbon nanofibers and related structures: controlled synthesis and directed assembly," *J. App. Phys*., vol. 97, pp. 041301 - 041301-39, 2005.
30. X. Yang, M. A. Guillorn, D. Austin, A. V. Melechko, H. Cui, H. M. Meyer III, V. I. Merkulov, J. B. O. Caughman, D. H. Lowndes, and M. L. Simpson, "Fabrication and characterization of carbon nanofiber-based vertically integrated Schottky barrier junction diodes," *Nano Letters*, vol. 3, pp. 1751–1755, 2003.
31. Q. Zhao, Z. Gan, and Q. Zhuang, "Electrochemical sensors based on carbon nanotubes," *Electroanalysis*, vol. 14, pp. 1609–1613, 2002.
32. S.-U. Kim and K.-H. Lee, "Carbon nanofiber composites for the electrodes of electrochemical capacitors," *Chem. Phys. Lett.*, vol. 400, pp. 253–257, 2004.
33. J. Jang, J. Bae, M. Choi, and S.-H. Yoon, "Fabrication and characterization of polyaniline coated carbon nanofiber for supercapacitor," *Carbon*, vol.43, pp. 2730–2736, 2005.
34. Y.-L. Yao and K.-K.Shiu, "A mediator-free bienzymaticamperometric biosensor based on horseradish peroxidase and glucose oxidase immobilized on carbon nanotube modified electrode," *Electroanalysis*, vol. 20, pp. 2090–2095, 2008.
35. M. Green and P. Hilditch, "Disposable single-use sensors," *Anal. Proc.* vol. 28, pp 374-376, 1991.
36. J. E. Frew and H. A. O. Hill, "Electrochemical biosensors," *Anal. Chem*., vol. 59, pp. 933A-944A, 1987.
37. J. Wang, "Modified electrodes for electrochemical sensors," *Electroanalysis*, vol. 3, pp. 255-259, 1991.

38. J. Wang and H. Wu, “Permselective lipid - poly(o-phenylenediamine) coatings for amperometricbiosensing of glucose,” *Anal. Chim. Acta,* vol. 283, pp 683-688, 1993.
39. Y. Degani and A. Heller, “Direct electrical communication between chemically modified enzymes and metal electrodes. I. Electron transfer from glucose oxidase to metal electrodes via electron relays, bound covalently to the enzyme,” *J. Phys. Chem.*, vol. 91, pp. 1285–1289, 1987.
40. Y. Xiao, F. Patolsky, E. Katz, J. F. Hainfeld, and I. Willner, “Plugging into enzymes: nanowiring of redox enzymes by a gold nanoparticle,” *Science*, vol. 299, pp. 1877-1881, 2003.
41. F. Patolsky, Y. Weizmann, and I. Willner, “Long-range electrical contacting of redox enzymes by SWCNT connectors,” *Angew. Chem. Int. Ed. Engl.*, vol. 43, pp. 2113-2117, 2004.
42. D. R. S. Jeykumari and S. S. Narayanan, “Fabrication of bienzymaticnanobiocomposite electrode using functionalized carbon nanotubes for biosensing applications,” *Biosensors and Bioelectron.*, vol. 23, pp. 1686-1693, 2008.
43. X. L. Luo, J. J. Xu, J. L.Wang, and H. Y. Chen, “Electrochemically deposited nanocomposite of chitosan and carbon nanotubes for biosensor application,” *Chem. Comm.*, vol.16, pp. 2169-2170, 2005.
44. T. Ruzgas, L. Gorton, J. Emneus, and G. Marko-Varga, “Kinetic models of horseradish peroxidase action on a graphite electrode,” *J. Electro. Chem.*, vol., 391, pp. 41-49, 1995.
45. L. Wu, X. Zhang, and H. Ju, “Amperometric glucose sensor based on catalytic reduction of dissolved oxygen at soluble carbon nanofiber,” *Biosensors and Bioelectron.*, vol. 23, pp. 479-484, 2007.
46. S-H Tark, A. Srivastava, S. Chou, G. Shekhawat, and V. P. Dravid, “Nanomechanoelectronic signal transduction scheme with metal-oxidesemiconductor field-effect transistor-embedded microcantilevers,” *Appl. Phys. Lett.*, vol. 94, pp. 104-101, 2009.
47. G. Sekhawat, S-H. Tark, and V. P. Dravid, “MOSFET-embedded microcantilevers for measuring deflection in biomolecular sensors,” *Science*, vol. 311, pp. 1592-1595, 2006.
48. P. M. Solomon, and H. Morkoc, “Modulation-doped GaAs/AlGaAs heterojunction field-effect transistors (MODFET’s), ultrahigh-speed device for supercomputers,” *IEEE Trans. Elec. Dev.*, vol. 31, pp. 1015-1027, 1984.
49. R. Dingle, H. Stormer, A. C. Gossard, and W. Wiegmann, “Electron mobilities in modulation doped semiconductor heterojunction superlattices,” *Appl. Phys. Lett*., vol. 31, pp. 665-667, 1978.
50. L. Esaki, and R. Tsu, “Superlattice and negative conductivity in semiconductors,” *IBM Internal Res. Rep.*, RC2418, 1969.
51. M. Morkoc, and P. M. Solomon, “The HEMT: A superfast transistor,” *IEEE Spectrum*, vol. 21, pp. 28-35, 1984.
52. M. A. Khan, A. Bhattarai, J. N. Kuznia, and D. T. Olson, “High electron mobility transistor based on a GaN-$Al_xGa_{1-x}N$ heterojunction,” *Appl. Phys. Lett.*, vol. 63, pp. 1214-1215, 1993.
53. L. F. Eastman, V. Talik, V. Kaper, J. Smart, R. Thompson, B. Green, J. R. Shealy, and T. Prunty, “Progress in High-Power, HIgh-Frequency AlGaN/GaN HEMTs,” *Phys. Stat. Sol.*, vol. 194, pp. 433-438, 2002.

54. S. A. Eliza, S. K. Islam, I. Lee, and E. Greenbaum, "Analysis of AlGaN/GaN HEMT modulated by photosystem I reaction centers," *Proceedings of International Semiconductor and Device Research Symposium*, College Park, MD, USA, 2007.
55. J. -K. Shin, D. –S. Kim, H. –J. Park, and G. Lim, "Detection of DNA and protein molecules using an FET-type biosensor with gold as a gate metal," *Electroanalysis*, vol. 16, pp. 1912-1918, 2004.
56. I. Lee, J. W. Lee, and E. Greenbaum, "Biomolecular Electronics: Vectorial Arrays of Photosynthetic Reaction Centers," *Physical Rev. Lett*., vol. 79, pp. 3294 – 3297, 1997.
57. P. R. Chitnis, "Photosytem I," *Plant Physiol.*, vol. 111, pp. 661-669, 1996.
58. I. Lee, J.W. Lee, A. Stubna, and E. Greenbaum, "Measurement of electrostatic potentials above oriented single photosynthetic reaction centers," *J. Phys. Chem. B*, vol. 104, pp. 2439- 2443, 2000.
59. J. Karczewski, M. Karczewski, M. Glyda and K. Wiktorowicz, "Role of TH1/TH2 cytokines in kidney allograft rejection," *Transplant. Proc*., vol. 40, pp. 3390-3392, 2008.
60. M.A. Cascieri and M. S. Springer, "The chemokine/chemokine-receptor family: potential and progress for therapeutic intervention," *Cur. Opin. Chem. Bio.*, vol. 4, pp. 420-427, 2000.
61. A. D. Luster, "Chemokines — chemotactic cytokines that mediate inflammation," *N. Engl. J. Med.*, vol. 338, pp. 436-445, 1998.
62. M. B. Auerbach, N. Shimoda, H. Amano, J. M. Rosenblum, D. D. Kish, J. M. Farber and R.L. Fairchild, "Monokine induced by Interferon-γ (MIG/CXCL9) is derived from both donor and recipient sources during rejection of class II major histocompatibility complex disparate skin allografts, " *Am. J. Pathol.*, vol. 176, pp. 2172-2181, 2009.
63. F. N. Lauw, A. J. H. Simpson, J. M. Prins, S. J. H. van Deventer, W. Chaowagul, N. J. White and T. van der Poll, "The CXC chemokines gamma interferon (IFN-γ)-inducible protein 10 and monokine induced by IFN-γ are released during severe melioidosis," *Infection and Immunity*, vol. 68, pp. 3888-3893, 2000.
64. J . J. Yun, M. P. Fischbein, D. Whiting, Y. Irie, M. C. Fishbein, M. D. Burdick, J. Belperio R. M. Strieter, H. Laks, J. A. Berliner, and A. Ardehali, "The role of MIG/CXCL9 in cardiac allograft vasculopathy," *Am. J. Pathol.*, vol. 161, pp. 1307-1313, 2002.
65. J. J. Gooding, P. Erokhin, D. Losic, W. Yang, V. Policarpio, J. Liu, F. M. Ho, M. Situmomorang, D. B. Hibbert, J. G. Shapter, "Parameters important in fabricating enzyme electrodes using self-assembled monolayers of alkanethiols," *Anal. Sci.*, vol. 17, pp. 3-9, 2001.
66. S. K. Arya, G. Chornokur, M. Venugopal, and S. Bhansali, "Dithiobis(succinimidyl propionate) modified gold microarray electrode based electrochemical immunosensor for ultrasensitive detection of cortisol," *Biosens. Bioelecton.*, vol. 25, pp. 2296-2301, 2010.
67. J. F. Cabrita, L. M. Abrantes, and A. S. Viana, "N-Hydroxysuccinimide-terminated self-assembled monolayers on gold for biomolecules immobilization," *Electrochim. Acta*, vol. 50, pp. 2117-2124, 2005.
68. D. Quan and W. Shin, "Modification of electrode surface for covalent immobilization of laccase," *Mater. Sci. Eng. C*, vol. 24, pp. 113-115, 2004.

69. P. Wagner, M. Hegner, P. Kerner, F. Zaugg, and G. Semenza, "Covalent immobilization of native biomolecules onto Au(111) via N-hydroxysuccinimide ester functionalized self-assembled monolayers for scanning probe microscopy," *Biophys. Jour.*, vol. 70, pp. 2052-2066, 1996.
70. D. L. Johnson, J. L. Thompson, S. M. Brinkmann, K. A. Schuller, and L. L. Martin, "Electrochemical characterization of purified Rhus vernicifera laccase: voltammetric evidence for a sequential four-electron transfer," *Biochemistry*, vol. 42, pp. 10229-10237, 2003.
71. Pierce technical datasheet, available online at: www.piercenet.com/products/browse.cfm?fldID=02030234.
72. M. Sela, E. Mozes, G. M. Shearer, and Y. Karniely, "Cellular aspects of the inverse relationship between the net charge of immunogens and of antibodies elicited," *Proceedings of the National Academy of Science*, vol. 67, pp. 1288-1293, 1970.
73. C. Wingren, U. B. Hansson, C. M. Magnusson, and M. Ohlin, "Antigen-binding sites dominate the surface properties of IgG antibodies," *Mol. Immunol.*, vol. 32, pp. 819-827, 1995.
74. O. Ambacher, J. Smart, J. R. Shealy, N. G. Weimann, K. Chu, M. Murphy, W. J. Schaff, and L. F. Eastman, R. Dimitrov, L. Wittmer, M. Stutzmann, W. Rieger and J. Hilsenbeck, "Two dimensional electron gases induced by spontaneous and piezoelectric polarization charges in N- and Ga-face AlGaN/GaN heterostructures," *J. Appl. Phys.*, vol. 85, pp. 3222-3233, 1999.
75. A. F.M. Anwar, E. W. Faraclas, "Schottky barrier height in GaN/AlGaN heterostructures," *Solid State Electron.*, vol. 50, pp. 1041-1045, 2006.
76. D. Delagebeaudeuf and N. T. Linh, "Metal-(n) AlGaAs-GaAs two-dimensional electron gas FET," *IEEE Trans. Elec. Dev.*, vol. 29, no.6, pp. 955-960, 1982.
77. A. Shey, and W. H. Ku, "An analytical current-voltage characteristics model for high electron mobility transistors based on nonlinear charge-control formulation," *IEEE Trans. Elec. Dev.*, vol. 36, pp. 2299-2306,1989.
78. C. S. Chang, and H. R. Fetterman,"An analytic model for high-electron mobility transistors," *Solid State-Electron.*, vol. 30, pp. 485-491, 1987.
79. S. M. Sze, "Physics of semiconductor devices," 2nd edition, 1981.
80. S. Vasudevan, K. Walczak, N. Kapur, M. Neurock, and A. W. Ghosh, "Modeling Electrostatic and Quantum Detectionof Molecules," *IEEE Sensors J.*, vol. 8, pp. 857-862, 2008.
81. M. Johansson, I. Lundström, and L.-G. Ekedahlb, "Bridging the pressure gap for palladium metal-insulator-semiconductor hydrogen sensors in oxygen containing environments," *J. Appl. Phys.*, vol. 84, pp. 44-51, 1998.

Vita

Fahmida S. Tulip (Student member, IEEE) received the received the B. Sc. Degree in electrical and electronic engineering from Bangladesh University of Engineering and Technology, Dhaka, Bangladesh in 2008.

She is currently pursuing her Ph. D. degree in the Department of Electrical Engineering and Computer Science, the University of Tennessee, Knoxville, USA. Her research interests include modeling and optimization of III-nitride semiconductor devices and micro- and nanostructured devices for sensor applications.